PREDICTION OF SURGE AND SWAB PRESSURE PROFILE FOR FLOW OF YIELD POWER LAW DRILLING FLUID MODEL THROUGH ECCENTRIC ANNULI

MBEE, OLEMAKPADU NELSON

DECEMBER 2011

PREDICTION OF SURGE AND SWAB PRESSURE PROFILE FOR FLOW OF YIELD POWER LAW DRILLING FLUID MODEL THROUGH ECCENTRIC ANNULI

A

THESIS

Presented to the Department of Petroleum Engineering

Of the African University of Science and Technology

In Partial Fulfillment of the Requirements

For the Degree of

MASTER OF SCIENCE

By

MBEE, OLEMAKPADU NELSON,

Abuja, Nigeria

December 2011.

PREDICTION OF SURGE AND SWAB PRESSURE PROFILE FOR FLOW OF YIELD POWER LAW DRILLING FLUID MODEL THROUGH ECCENTRIC ANNULI

By

MBEE OLEMAKPADU NELSON

RECOMMENDED: ----------

Advisory Committee Chair

Department Head

APPROVED: ----------

DEDICATION

To my perfect life complement, Temitope Eluyemi

ACKNOWLEDGMENTS

I would like to express my sincere gratitude to my advisor and thesis committee chairman, Prof. Godwin A. Chukwu, for his guidance, encouragement and support throughout the course of this work. But for his invaluable supervision, this work would not have materialized. I also want to thank Dr Alpheus Igbokoyi, and Prof. S.Osisanya for their contribution as the members of my thesis committee and for their suggestions and support throughout the work. I also want to thank Prof. Wesley Pacheco Calixto for his immense contribution as well.

I also wish to profoundly acknowledge the financial support of the Petroleum Technology Development Fund, PTDF, for providing me with a full scholarship to study at the African University of Science and Technology, without their funding of this course, this work wouldn't have materialized as well.

I also wish the recognize the support of the visiting Professors to the University for their course lectures in Petroleum Engineering and most importantly the motivation and inspirations I have received from them and also to my friends for making stay at the University a memorable one, and also to members of the AUST-Nucleus group.

I would like to give special appreciation to my family, my dad Nelson Mbee, my mum Omonaa Mbee. My siblings Olemabu Mbee, Kafonya Mbee, Ere Mbee and Maama Mbee for their moral support. I also want to recognize Jollytine Oyakhire for his long time friendship and to Isaac Nwokocha for always being a friend. Finally I would like to thank God Almighty who owns all of life, power, ideas, wisdom and knowledge. His love keeps me every day by day, year in and out to learn more of Him.

ABSTRACT

Surge and swab pressure computation is very important in drilling hydraulics. Most blowout problem in oil wells have been as a result of surge and swab pressures developed from running or pulling of tubular goods in liquid-filled bore hole. Excessive surge pressures can fracture the geological formation, while excessive swab can result in blowouts. In this work the analysis of steady state, laminar couette flow of non-Newtonian yield power law drilling fluid model (Herschel-Bulkley) is used to compute the surge and swab in Eccentric annuli.

A slot flow model was first of all developed for a yield power law fluid in a concentric annulus, this model equation formed the basis of this work. And in solving for an eccentric annulus, the mathematical concept of conformal mapping was applied. A suitable mathematical bilinear function was applied in mapping the original eccentric plane, for a particular eccentricity ratio, to a concentric (zero eccentricity ratio) plane.

By applying a suitable iterative technique the various pressure values were obtained and plots of dimensionless pressures versus dimensionless flow rate or radii were made. From which for a particular eccentricity ratio, fluid behavior index, shear stress and consistency index, the corresponding surge or swab can be obtained.

LIST OF FIGURES

LIST OF TABLES

NOMENCLATURE

ε = Eccentricity ratio

c = concentric radial clearance ($r_2 - r_1$), in. (mm)

d_2 = Outer-Pipe or hole diameter, in. (mm)

d_1 = Inner-Pipe (drill Pipe) diameter, in. (mm)

r_2 = Outer-pipe or hole radius, in. (mm)

r_1 = Inner-pipe (drill pipe) radius, in. (mm)

n = Fluid index behavior, dimensionless

b = Constant, dimensionless

τ_0 = Yield Stress, lbf/100 ft^2 (Pa)

K = Power-law consistency behavior, lbf-sec^n/100ft^2 (Pa.s^n)

e = inner-pipe offset distance relative to hole center, in. (mm)

ρ_2 = Mapped concentric hole radius, in. (mm)

ρ_1 = Mapped concentric inner-pipe radius, in. (mm)

a = Real positive constant for bilinear transformation, in^{-1}. (mm^{-1})

$\widetilde{q_t}$ = Dimensionless total flow rate, dimensionless

$\tilde{y}$ = Dimensionless distance, dimensionless

ΔP = Pressure drop, psi (Pa)

L = Length of drill pipe in liquid filled bore hole, in. (mm)

P = Dimensionless Pressure, dimensionless

V_p = Velocity of the drill pipe, fps (mm/s)

$\boldsymbol{\phi}$ = Dimensionless term, dimensionless

TABLE OF CONTENTS

CHAPTER ONE

INTRODUCTION

1.0 INTRODUCTION:

This study covers Non-Newtonian fluid flow in eccentric annulus, with special case study to Yield Power Law Drilling Fluid Model. The Yield Power law drilling fluid model considered here is the yield pseudo plastic (Herschel Buckley Model), where the fluid index behavior is less than one. The Herschel Buckley Model is used to commonly represent the behavior of drilling fluids.

1.1 BACKGROUND OF THESIS:

There is much relevance in the study of surge and swab in bottom hole while drilling. A surge is an increase in the bore hole hydrostatic pressure as a result of increasing velocity of the drill string down hole. This can create a pressure that can fracture the formation, that is, if the resultant hydrostatic pressure exceeds the fracture pressure of the formation. In lowering the drill string in a mud filled hole, great care is taken so that a surge doesn't occur. A surge can lead to lost circulation, whereby mud used in drilling is lost into the formation.

On the converse, a swab can occur while pulling out the drill string or tubular goods. As a result of pulling, a partial vacuum is created and as "Nature abhors a Vacuum" formation fluid from the pores of the formation would take up place to replace the vacuum. This can result to a Kick and if not controlled can result to a blow out, which is an uncontrollable outpour of formation fluid and drilling mud fluid from the hole.

As a result of the phenomenon of surge and swab, great care has to be taken to prevent the adverse effects of it. The question then becomes, what are the best ways surge and swab can be quantified? At what values of pressure is it going to fracture the formation? And also at what values can a kick occur? And also at what values of velocity would it be safe to lower or raise tubular goods or drill string? These questions led to research and computational work resulting in generation of pressure profiles for different fluid models. Plots are also made using dimensionless characteristics. With these charts it is very easy to read up a particular pressure surge value for a corresponding velocity value, and with such a value, care is taken so as not to exceed such values. These can be applied on the field.

1.2 SCOPE

This work would be combining a fluid flow model, a flow phenomenon in a physical situation to solve another physical problem. Here the fluid type is a Non-Newtonian Yield Power Law fluid model, and would be applying couette flow phenomenon. Couette flow is the phenomenon whereby fluid is confined between two coaxial cylinders, one of which is stationary and the other is moving at a uniform velocity. This flow characteristic is representative of flow in the wellbore annulus where the wall of the wellbore is represented by the stationary cylinder and the drill string or casing pipe is represented by the moving cylinder. The fluid average velocity is dependent on the velocity of the moving cylinder (Akrong, 2009).

The physical situation that would be observed in this work is Eccentricity. Majorly, in all drilling problems involving drill string or tubular goods in wellbore, concentricity is assumed, but this is not actually so. In concentricity it is assumed that the drill string is centrally placed in the

wellbore, such that it has the same uniform clearance. But in actual drilling practice, this is not so, the drill string is not centrally placed but it tends more towards a particular side of the wellbore. A pipe can have an eccentricity of 100%, ε=1.0, that is, the pipe touches on the side of the hole and it could also be 50%, that is ε=0.5, 80% or ε=0.8 and eccentricity, ε, could also be 0%, ε=0.0, that is the pipe is centrally placed hence concentric. In this work couette flow analysis would be used.

1.3 PROBLEM STATEMENT

With the resulting explanation of surge and swab pressures phenomenon for couette flow, and the attendant situation of eccentricity of pipe in wellbore, there is need to compute the surge or swab pressure values combined for various eccentricity ratios for a yield Power law drilling fluid model. The computed surge would be used as a check so as not to exceed the fracture gradient of the formation. This would then prevent lost circulation of the drilling mud. Also the computed swab pressure value can be used as a check so as not to go below the formation pore pressure. This would then prevent kicks or blowouts.

1.4 OBJECTIVES

The objectives of this work are to use Yield Power Law Drilling fluid Model:

1) To confirm formula for slot flow model for yield Power law fluid for concentric annulus using couette flow analysis.

2) Compute the surge or swab Pressure value for Yield Power Law fluid, for varying eccentricity ratios.
3) Develop a Program that computes the surge/swab pressure value for any field combination of eccentricity ratio, and yield power law fluid parameters.

1.5 METHODOLOGY

The methodology is to develop the slot model for concentric annulus for a yield power law fluid and then applying the concept of conformal mapping, and then map the eccentric annulus, which is to be solved, into a concentric annulus.

With the already developed formulation, the mapped concentric annulus is then solved and a program that can easily solve for any field value combination is developed.

CHAPTER TWO

THEORY AND LITERATURE REVIEW

The study of fluid flow stems basically from the branch of fluid mechanics called hydraulics. This is the branch of engineering or science that studies the movement of fluids and the forces exerted by and on them. (Chukwu 2009).

2.1 Review of Fluid Classification

A fluid is basically defined as a substance that undergoes shear rate no matter how small upon the application of a shear stress. From the definition above the related parameters related above are shear stress and shear rate. Hence we expect some form of displacement (shear displacement) in the fluid. Fluids can be characterized in behavior based on the rheology or deformation behavior using rheological models. Rheology is defined as the "deformation of matter" or the study of relationship between applied forces (shear stress) at different shear rates.

2.1.1 Mathematical Models

A mathematical description of the relation between shear stress and sheer rate and viscous forces present in the fluid is required for the development of friction loss equations. The rheological models generally used to characterize fluid behavior are: (Adam et al, 1986)

a) Newtonian Model

b) Power Law Fluid Model

c) Bingham Plastic Fluid Model

a) **Newtonian Model**:

In this model, the shear stress is directly proportional to the shear rate. The constant of proportionality is known as the effective fluid viscosity. The mathematical formula for the Newtonian fluid is given by:

Shear stress (τ) = Viscosity (μ) x Shear Rate (γ) (1)

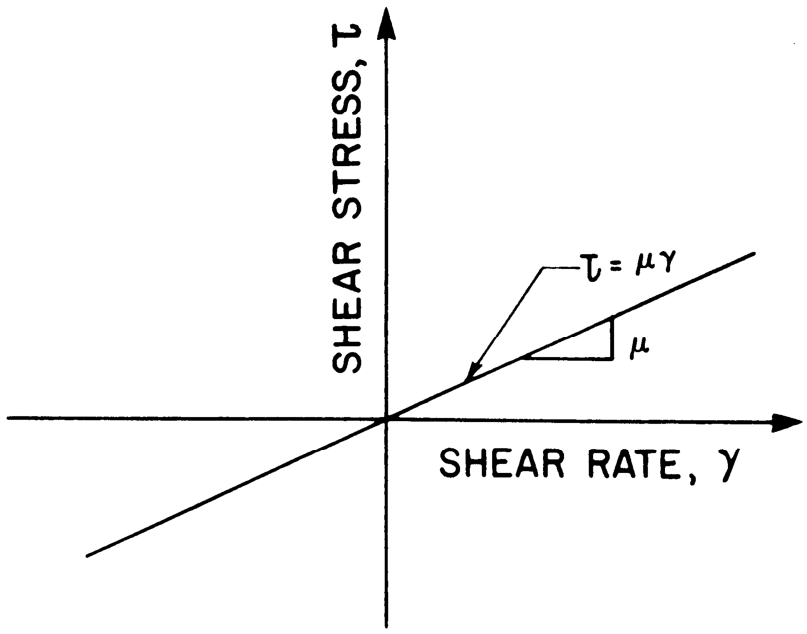

Figure 1**:** Shear stress Vs Shear rate for a Newtonian fluid

In the figure above the shear stress is directly proportional to the shear rate for a Newtonian fluid and the slope of the graph is the true or effective viscosity. Physical examples of fluid in this model are water, gases, kerosene, high gravity oils.

b) Power Law Fluid Model (Non-Newtonian Model)

The relationship between shear stress and rate is a non-linear. The fluid could be shear rate dependent. If the apparent viscosity decreases with increasing shear rate, then the fluid is termed pseudo plastic, and is dilatant if the apparent viscosity increases with increasing shear rate. For both cases the fluid is also called Non-Newtonian Model. The fluid can also be classified with respect to shear rate time dependency and it is thixopetric, if the apparent viscosity decreases after it has increased to a new constant value and could also be rheopectic, if the apparent viscosity increases after it must have increased to a new constant value.

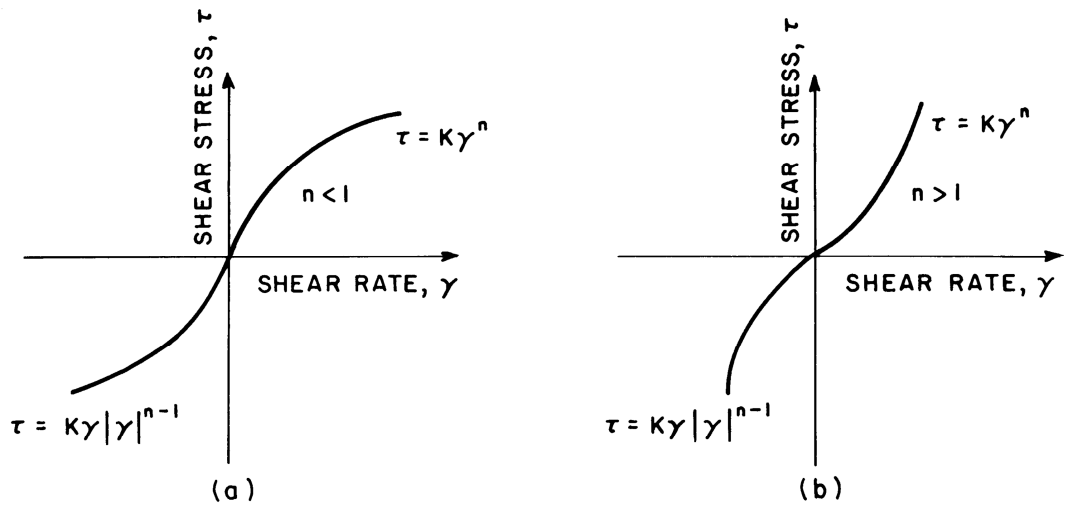

Figure 2**:** Shear stress Vs Shear rate a for power law fluid: (a) pseudo plastic (b) dilatant

The profiles in the figure above describe relations for shear stress versus shear rate for a non-Newtonian power law fluid. The profiles are curved unlike the Newtonian fluid which is a straight line. If the slope, which is a measure of the apparent viscosity, is taken at each point on the curve in (a), the slope would be decreasing for increasing shear rate, hence it is termed pseudo plastic and the slope in (b) would be increasing with increasing shear rate, hence termed dilatant. Note also that for $n<1$, the fluid is pseudo plastic and for $n>1$, the fluid is dilatant.

The power law model can be represented mathematically as:

$$\tau = k\gamma^n \qquad (2)$$

c) Bingham Plastic Model

This is a model used to characterize fluids that would not flow until the applied shear stress exceeds a certain minimum value τ_y , known as the yield stress. After this point the stress is then directly proportional to the shear rate.

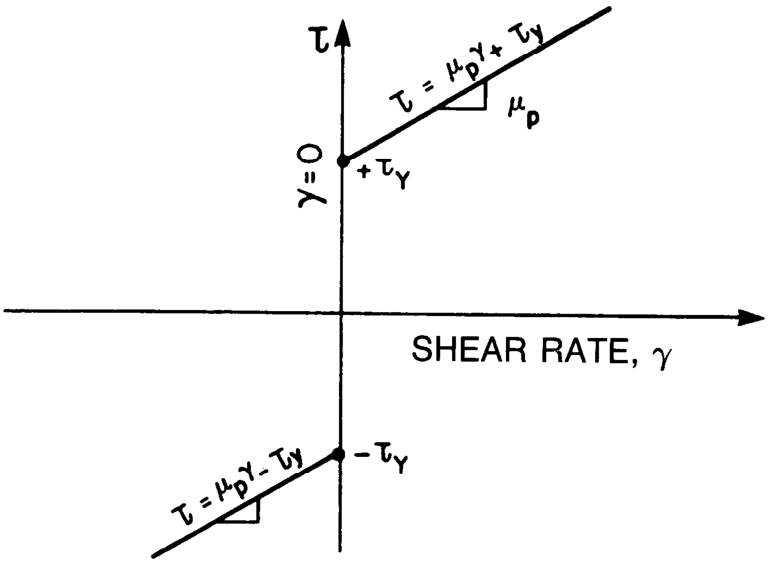

Figure 3**:** Shear Stress Vs Shear rate for a Bingham plastic fluid

In the figure above, the line does not start at the origin but at a particular shear stress value, $+\tau_y$, where the shear rate is zero. And the slope of the line is the plastic viscosity given as μ_p.

This model formula is given:

$$\tau=\tau_y + \mu_p(\gamma) \qquad (3)$$

Though there are other models such as Herschel Buckley, Robertson-Stiff, Casson model. These other major models have been developed which at low shear rates, exhibit behavior intermediate between that of the Bingham and Power-law models. These models are defined by:

(d) $\tau = \left[\tau_o^{1/2} + (\mu_p \dot{\gamma})^{1/2}\right]^2$ ..... (CASSON MODEL) (4)

(e) $\tau = K(\gamma_o + \gamma)^n$ .....(Robertson-stiff model) (5)

(f) $\tau = \tau_o + K\dot{\gamma}^n$ .....(Herschel-Buckley model) (6)

2.2 LITERATURE REVIEW

Study of surge and swab pressure is very important in the drilling industry; hence there has been much work in the subject area. In 1934 Canon described the changes in hydrostatic pressure due to withdrawing drill pipe from the hole. He predicted that swab pressure from pipe swabbing could be a cause of fluid influx and caused blowouts as well. The paper discussed the factors that affect the magnitude of pressure drops when drill pipe is withdrawn from hole. Such factors include the effect of high gel strength which resulted to high pressure drop, effect of mud weight, viscosity, the effect of relation of depth which showed that the pressure drop due to withdrawing the drill pipe is proportional to the length of drill pipe in the hole, effect of rate of withdrawal, effect of drainage, effect of annular space and so on.

In 1951 Goins et al studied the down-the-hole pressure surges and their effect on loss of circulation, the study also described pressure surges resulting from running pipes which resulted in rapidly breaking circulation which then caused lost circulation. He identified surges caused from running pipe, spudding while pumping, rapidly opening pumps to start circulation. He reported that surges may be avoided through slowed rates of pipe movement and slow breaking of circulation.

A study by Horn in 1951 showed that of the 55 California blowouts, 9 gave strong evidence that blowouts were caused principally by the reduction in static pressure during pipe withdrawal.

Cardwell in 1953 looked at the pressure changes in drilling well caused by pipe movement. He pointed out that many blowouts that occur in drilling operations where as a result of reduction in static pressure during drill pipe withdrawal.

Ormsby in 1954 developed a detailed analysis of the theory of pressure surges. He discussed both laminar and turbulent flow regimes of drilling fluid. Clark in 1955 presented graphs of surges and gave the equations to predict their magnitudes. He also considered pressure variation arising from viscous drag and inertial effects and also looked at a graphic view of Pressure Surges and Lost circulation. He concluded that there are very few natural combinations of geostatic and hydrostatic gradients that cannot be successfully drilled provided operators are willing to put forth the time and effort required for proper mud control.

Burkhardt in 1961 explained wellbore pressure surges produced by pipe movement. He made measurements of surge values from wellbore and made comparison of measured results with those predicted by the calculation. In his work the theory correctly predicts the existence and magnitude of various positive and negative peaks due to gel breaking, inertia and viscous drag of the mud. And that when running drill pipe or casing without fill-up devices, the surge due to viscous drag is usually the largest. In 1974 Fontnot and Clark presented an improved approach to help calculate down-hole pressures in a drilling well. The fluid properties were compensated with their variation with depth. A computer program was developed to compare the values obtained with experimental data. Also in 1974 Moore defined the three major causes of surge and swab pressure as; Viscous shear, breaking of gel strength and pipe acceleration or

deceleration (inertia). He also presented an equation to calculate the surge pressure required to break the gel strength.

In 1988 Mitchell presented a paper on dynamic surge/swab pressure predictions. He extended the surge/swab model to include features as (1) Pipe annulus and annulus pressures coupled through pipe elasticity (2) longitudinal pipe elasticity and fluid viscous forces to determine pipe displacement (3) Fluid properties that would vary as a function of temperature and pressure (4) Formation elasticity, pipe elasticity, and cement elasticity to determine the response of the well bore. He compared the constructed dynamic surge/swab model with experimental data and there was a good agreement.

Deniz in 1989 studied the flow of a power-law fluid in an eccentric annulus, he modeled the eccentric annulus as a slit of variable height and he also compared the volumetric flow rate of power-law fluid in the eccentric annulus with that of a concentric one for the same pressure drop. His study showed an increase in volumetric flow rate for an eccentric case.

Yuejin and Peden in 1990 studied the flow of Non-Newtonian fluids through eccentric annuli. The study was for laminar eccentric annular flow. The eccentric annulus was represented by an infinite number of concentric annuli of variable radii. The authors obtained analytical solutions for stress, shear rate, velocity and volumetric flow rate for both Bingham plastic and Power law fluids.

Fredrickson and Bird (1960) derived an analytical solution for steady state axial flow of Non-Newtonian fluids in a long cylindrical annulus, but the model is limited to concentric (perfectly centered) inner pipe. Haciilamoglu and langlinais in 1991 studied the effect of pipe eccentricity

on pressure surges, and they discovered as the eccentricity increased the pressures surges reduced and that concentricity over predicted the value of the surge pressures.

Bizanti (1991) in a paper, “Are Improved Surge Models Needed? ”, compared existing surge models obtained from steady state. In the paper, he concluded that the steady-state surge models over-predict surge pressures for high yield point muds and it under-predicts surge pressures for high mud weights in deep wells. Chukwu and Blick in 1991 gave theoretical results of surge and swab pressures for couette flow of power law fluids through concentric annulus and a graphical technique was used to easily compute the surge and swab pressure from a family of curves for different pipe/hole diameter ratios for field applications.

Chukwu in 1995 developed a practical approach for predicting casing running speed from Couette Flow of Non-Newtonian Power-Law Fluids. He made an analysis of steady laminar couette flow of Non-Newtonian Power law fluids through concentric annular wellbore and employed the computed surge pressures, in combination with family of curves to determine the maximum velocities at the which the casing pipes can be run in the hole without the danger of fracturing the formation.

Rubiandini (2000) described new formula of surge pressure for determining safe trip velocities. He basically calculated the surge/swab value from existing equations, but introduced a correction factor, which is a function of a combination of mud properties, pipe and hole sizes, correction parameter factor of plastic viscosity, yield point, mud density and hole-pipe size. He prepared a computer program for the new formula for surge.

Ramadan (2005) described experimental study and modeling of Yield-Power-law fluid flow in pipes. He studied the effects of pipe eccentricity, diameter ratio and fluid rheology on friction pressure loss and carried extensive flow experiments with polymer-based fluids. He computed pressure loss in eccentric annuli using three hydraulic models and compared the models with experimental measurements.

Ozbayoglu in 2006 made analysis of the effect of eccentricity on flow characteristics of annular flow of Non-Newtonian fluids using Finite Element Method (FEM). His results showed that as eccentricity increased FEM estimate of the frictional pressure losses were more accurate than conventional methods. He pointed out that as eccentricity increases, frictional pressure losses decreases, and this was validated from simulation and as well as from experiments. He observed the velocity profiles of any cross section of the wellbore using FEM with a realistic projection.

In 2010 Freddy Crespo looked at Surge and Swab Pressure Predictions for yield-Power-law Drilling Fluids. He showed that the pressure surge depends strongly on drill pipe tripping speed, wellbore geometry, flow regime, fluid rheology and whether pipe is often open or closed. He concluded that surge/swab pressure is also attributed to different flow phenomena including pipe eccentricity, geometric irregularities, acceleration and dynamic effects.

CHAPTER THREE

DEVELOPMENT OF MODEL EQUATIONS

In developing the equations for flow of yield power law in eccentric annulus, the geometry consists of two cylinders. The smaller inner cylinder represents the tubular goods and the larger outer cylinder represents the hole. This is represented by a cross section of two circles and the eccentric case does not have circles with the same centre, but they lie on the same straight line axis. The inner cylinder moves with a uniform velocity.

The following assumptions were made in development of the equations:

1.) Single phase, steady state incompressible fluid flow.
2.) The flow regime is considered laminar.
3.) The flow is isothermal that is the temperature of the fluid is constant, and also with constant fluid properties.
4.) Gravitational and slip effects are not considered.
5.) The inner cylinder moves with at a constant speed Vp.
6.) Consideration is for a closed pipe system. The inner pipe end is sealed.
7.) Couette flow phenomenon is assumed.

3.1 FORMULATION FOR ECCENTRIC HEIGHT IN ECCENTRIC ANNULUS

This is a review formulation for Eccentric Height, h

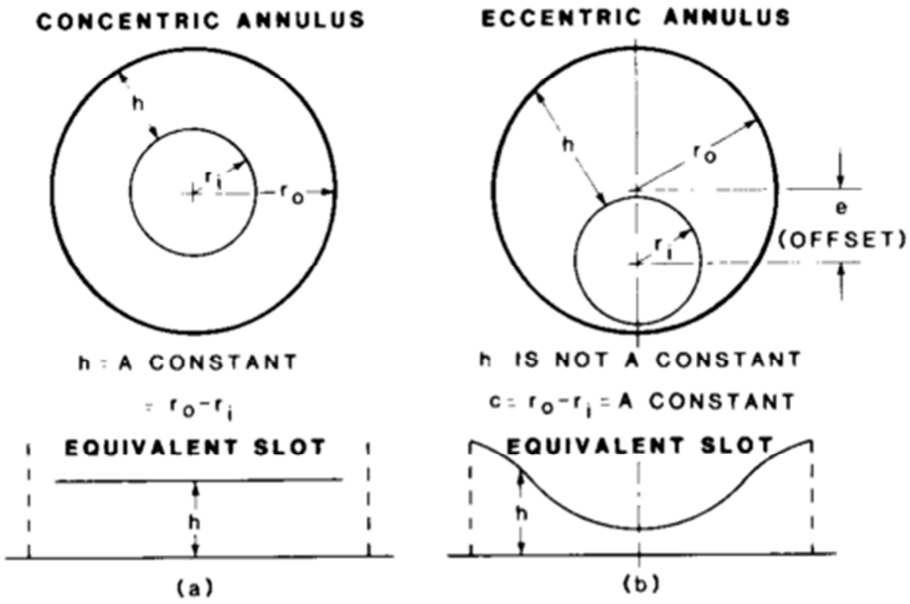

Figure 4: Cross section for Concentric and Eccentric Annulus, with corresponding equivalent slot models (A.W. Iyoho et al 1981)

The figure 4 above shows the cross section for concentric annulus which has a uniform clearance and that for an eccentric annulus which has a varying clearance.

Given an outer-pipe or hole radius of r_O and outer or inner pipe radius of r_i, for a concentric annulus the radial clearance, c, is uniform. Hence h is also constant.

$$h = c = H = r_o - r_i \tag{7}$$

But for an eccentric annulus which is the case study of this work, h, varies around the circle. Depending on the nomenclature for angle notation, it starts from a maximum then approaches an average concentric value, reaches a minimum and then back to the average, and back to the maximum value. The distance between the centers of both circles which is called the offset distance, e. Also the eccentricity ratio, ε, is the ratio of offset distance to radial clearance. For a concentric case the offset distance is zero, both circles have the same centers and the eccentricity ratio is also zero.

Hence for an eccentric case, the eccentricity ratio:

$$Eccentricity\ ratio, \varepsilon = \frac{offset\ distance, e}{Radial\ Clearance, c} = \frac{e}{(r_o - r_i)} = \frac{e}{c} \tag{8}$$

Therefore,

$$e = c\varepsilon \tag{9}$$

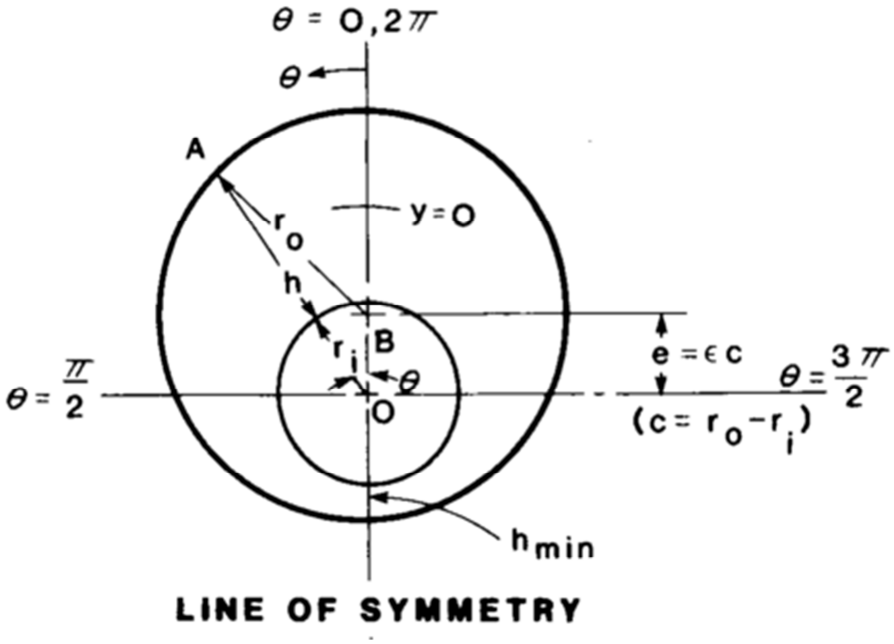

Figure 5: Nomenclature for Eccentric Annulus (A.W.Iyoho et al 1981)

In the figure 5 above shows the varying eccentric height and the notation for the angle used is such that the angle is taken as moving anti-clockwise from the North.

It is of interest here to review the formulation for h, for eccentric case:

Extracting the triangle ABO from figure above:

Figure 6: Extracted Triangle from Nomenclature of Eccentric Annulus

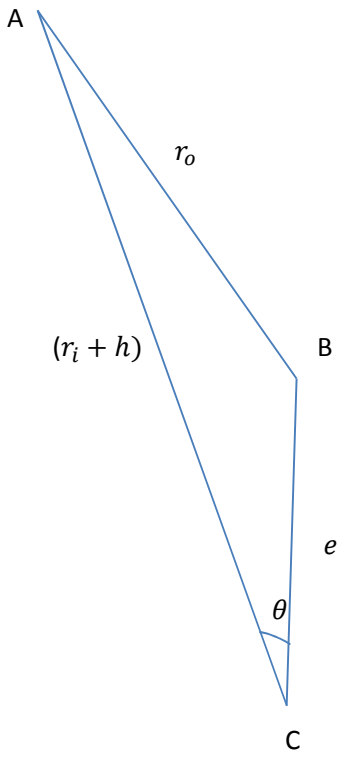

By applying cosine rule on the figure 6

$$r_o^2 = (r_i + h)^2 + e^2 - 2(r_i + h)eCos\theta \quad (10)$$

$$r_o^2 = r_i^2 + 2r_i h + h^2 + e^2 - 2r_i eCos\theta - 2heCos\theta \quad (11)$$

Rearranging:

$$h^2 + 2h(r_i - eCos\theta) + (e^2 - r_o^2 + r_i^2 - 2er_iCos\theta) = 0 \qquad (12)$$

Solving the quadratic equation (5) for h, using the quadratic formula;

$$h = \frac{2(eCos\theta - r_i) \pm \sqrt{[4(r_i - eCos\theta)^2 - 4(e^2 - r_o^2 + r_i^2 - 2er_iCos\theta)]}}{2} \qquad (13)$$

Simplifying

$$(r_i - eCos\theta)^2 - (e^2 - r_o^2 + r_i^2 - 2er_iCos\theta)$$

$$= r_i^2 - 2r_iCos\theta + e^2Cos^2\theta - e^2 + r_o^2 - r_i^2 + 2r_iCos\theta \qquad (14)$$

$$= e^2Cos^2\theta - e^2 + r_o^2 = r_o^2 - e^2(1 - Cos^2\theta) = r_o^2 - e^2Sin^2\theta \qquad (15)$$

This becomes the expression in the square root sign, therefore back to Equation (13)

$$h = (eCos\theta - r_i) \pm (r_o^2 - e^2Sin^2\theta)^{0.5} \qquad (16)$$

Taking the positive root value, and also applying Equation (9) (Iyoho, et al, 1981)

$$h = (r_o^2 - \varepsilon^2c^2Sin^2\theta)^{0.5} - r_i + \varepsilon cCos\theta \qquad (17)$$

Equation (8) is the variation of eccentric height in an eccentric annulus and it is the fundamental basis for this work. This definitely shows that the height varies with angle of rotation and is not uniform like in concentric annular case. Hence h is a function of the

clearance, angle and eccentricity ratio. But for a particular drilling geometry, there is a particular r_o, r_i, and off course eccentricity ratio, ε, the angle largely varies while drilling.

Note, h, is maximum at θ=0, in Equation (17), is zero and:

$$h = (r_o^2 - \varepsilon^2 c^2 Sin^2 0)^{0.5} - r_i + \varepsilon c Cos 0 \quad (18)$$

$$h = (r_o - r_i) + \varepsilon c = c + \varepsilon c \quad (19)$$

Applying Equation (7) to Equation (19)

$$h_{max} = (1 + \varepsilon)H \quad (20)$$

And h is minimum at θ=180^o or π radians.

$$h = (r_o^2 - \varepsilon^2 c^2 Sin^2 \pi)^{0.5} - r_i + \varepsilon c Cos \pi$$

$$h = (r_o - r_i) - \varepsilon c = c - \varepsilon c$$

And from applying Equation (7) to Equation (19)

$$h_{min} = (1 - \varepsilon)H \quad (21)$$

do(in)	di(in)	ro(in)	ri(in)	c(in)	ε	e(in)
10.00	7.00	5.00	3.50	1.50	0.50	0.75

Table 1: Hole geometry for an eccentricity ratio, ε=0.5

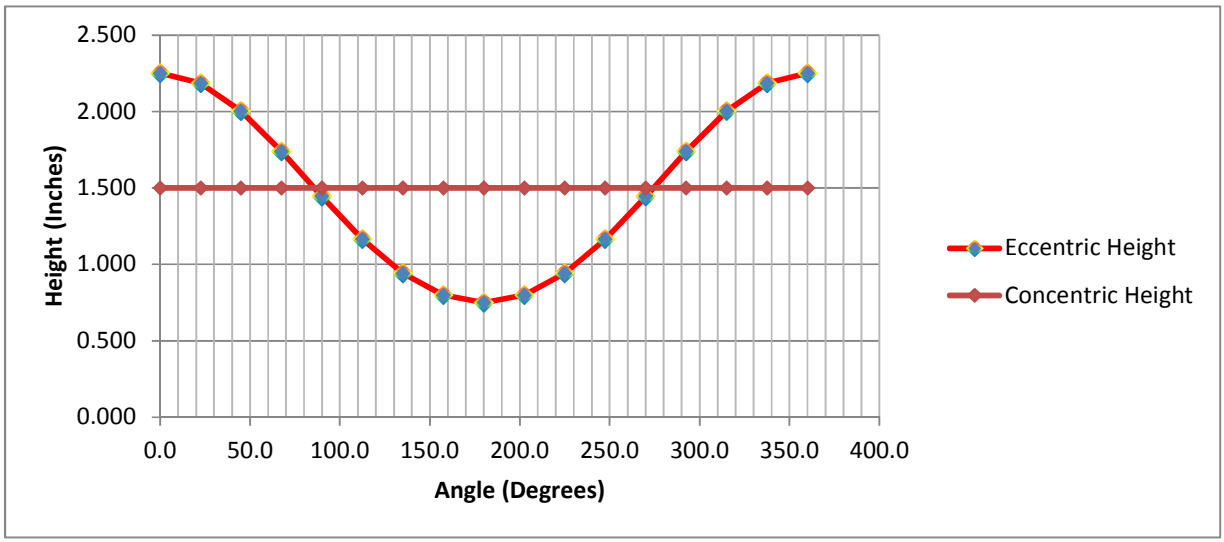

Figure 7: Comparison between Eccentric Heights for Concentric and Eccentric Annulus

By assuming some real values for hole diameter and tubular diameter as shown in Table 1 above for an eccentricity ratio of 0.50, and for varying angle from 0 to 360 degrees, and by

substituting into equation (18), the height for concentric and eccentric case is plotted, and the variation is shown in figure 7.

From this section the eccentric height is seen to vary as in equation (18) and the key idea in the methodology of this work was to seek, a function that would transform the varying slot height into a uniform one.

3.2 ANALYSIS OF SLOT FLOW MODEL OF POWER LAW AND YIELD POWER LAW DRILLING FLUIDS FOR CONCENTRIC ANNULUS

Following the methodology of this thesis, which is first to map the eccentric annulus from the z plane to concentric annulus and then to use the slot model to solve for the resultant concentric annulus. Hence it is of importance to study the analysis of surge and swab of fluids using the slot model. One of such work of importance is by Chukwu and Blick (1989), and it was developed for power law fluids.

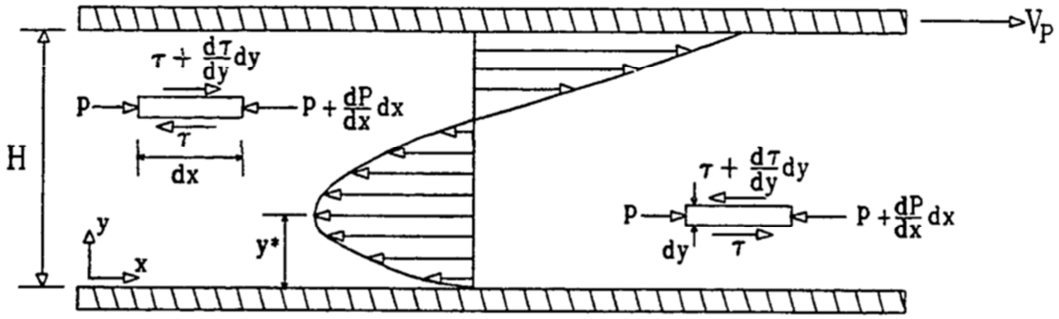

Figure 8: Geometric Parameters for a Power law fluid flow through slot (Chukwu and Blick 1989)

3.2.1 ANALYSIS OF FORMULATION FOR SLOT MODEL FOR POWER LAW FLUIDS

In figure 8 accounts for fluid displacement, and so the fluid region is separated into two different regions. Region I, a sheared region which is to the left of the figure and another sheared region II which is to the right of figure. Chukwu and Blick (1989) obtained the following dimensionless velocity profiles:

$$\widetilde{U_1} = \boldsymbol{P}\{[\tilde{y}^* - \tilde{y}]^b - [\tilde{y}^*]^b\} \tag{22}$$

$$\widetilde{U_2} = 1 - \boldsymbol{P}\{[1 - \tilde{y}^*]^b - [\tilde{y} - \tilde{y}^*]^b\} \tag{23}$$

For regions 1 and 2 for the fluid profiles in figure 8 above.

An identity equation was obtained by equating the velocities in both equations (22) and (23) to obtain the equation below for power law fluids:

$$(1-\tilde{y}^*)^b - (\tilde{y}^*)^b - \frac{\mathbf{1}}{\boldsymbol{P}} = \mathbf{0} \quad (24)$$

Chukwu and Blick (1989) stated that the equation above can be solved by iteration or by Modified Newton-Raphson**.**

They also obtained dimensionless flow rate with solution of $\tilde{y}^*$,from Equation (24) at assumed dimensionless pressure gradient ,**P**.

$$\widetilde{Q_T} = \widetilde{Q_1} + \widetilde{Q_2} = -\boldsymbol{P}\left(\frac{b}{b+1}\right)(\tilde{y}^*)^{b+1} - [\boldsymbol{P}(1-\tilde{y}^*)^b - 1][1-\tilde{y}^*] + \boldsymbol{P}\left(\frac{1}{b+1}\right)(1-\tilde{y}^*)^{b+1} \quad (25)$$

$$b = \frac{1+n}{n} \quad (26)$$

$$\boldsymbol{P} = \left(\frac{n}{n+1}\right)\left(\frac{H}{V_p}\right)\left(\frac{\Delta P}{LK}\right)^{1/n} \quad (27)$$

The dimensionless regional velocities for regions I and II are given by equations (28) and (29)

$$\widetilde{U_1} = \frac{U_1}{V_p} \quad (28)$$

$$\widetilde{U_2} = \frac{U_2}{V_p} \quad (29)$$

Chukwu and Blick (1989) did the formulation for power law fluids for concentric annulus, and a key variable was the dimensionless flow rate which served as an input to read the profile

charts. But the fluid of interest here is yield power law drilling fluid. So a similar formulation for yield power law drilling fluid would be of relevance.

3.2.2 FORMULATION OF SLOT MODEL FOR YIELD POWER LAW FLUIDS

The formulation for yield Power law fluid which uses the similar approach as Chukwu and Blick (1989) above, was developed from the work by Crespo and Ahmed (2010). The formulation by Crespo and Ahmed (2010) was done for yield Power law fluid, which suits the purpose of this work. The work considers the flow of yield Power law fluid, with an inner pipe diameter, dp, been pulled out with a velocity, Vp from a hole diameter dh.

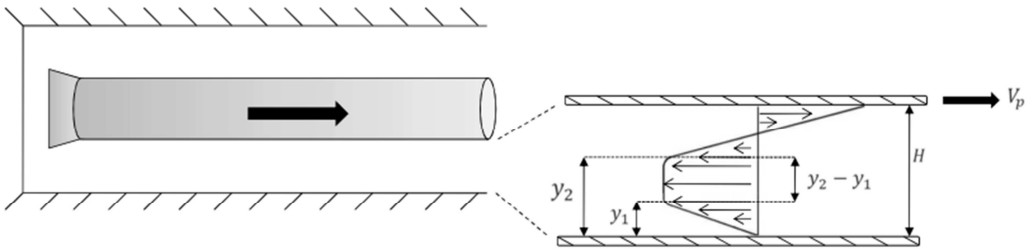

Figure 9: Slot model representation of a Yield Power Law Fluid of a Concentric Annulus. (Crespo and Ahmed 2010)

According to Crespo and Ahmed, the annular velocity profile during tripping operations would be made of three regions as illustrated in figure 9.

i) Outer Sheared Region, Region I, with boundary limits $0 \leq y \leq y_1$

ii) Plug Zone, Region II, with boundary limits $y_1 \leq y \leq y_2$

iii) Inner Sheared Region, Region III, within boundary limits $y_2 \leq y \leq H$

Fluid with in the inner sheared region, which is close to the moving wall or drill pipe moves in the direction of the upper plate. Figure 10 clearly shows the velocity profile with the corresponding boundary limits.

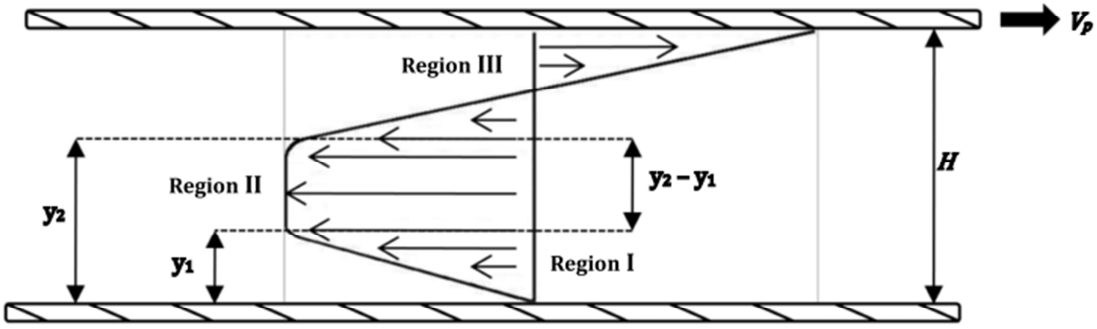

Figure 10: Velocity Profile of Yield Power law through a slot of a concentric annulus. (Crespo and Ahmed 2010)

The formulation for the yield Power law fluid here is done with comparison to that by Chukwu and Blick (1989).

3.2.3 Velocity Profile Development for Region I: $0 \leq y \leq y_1$

From figure 11 consider a fluid element being acted upon by the forces shown below.

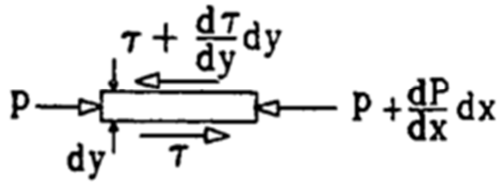

Figure 11: Pressure and shear stress forces on yield power law fluid element in region 1

$$\overrightarrow{\sum F_x} = 0 \tag{30}$$

Summing the net forces in the x direction

$$Pdy - \left(P + \frac{dP}{dx}dx\right)dy + \tau dx - \left(\tau + \frac{d\tau}{dy}dy\right)dx = 0 \tag{31}$$

$$-\frac{dP}{dx}dxdy - \frac{d\tau}{dy}dydx = 0 \tag{32}$$

Dividing both sides of equation (32) by , have

$$-\frac{dP}{dx} = \frac{d\tau}{dy} \tag{33}$$

Integrating both sides of (33) with respect to y, within the boundary limits of region I;

$$-\frac{dP}{dx}\int_0^y dy = \int_{\tau_w}^{\tau}\frac{d\tau}{dy}dy \tag{34}$$

Let $\frac{dP}{dx} = \frac{\Delta P}{L}$ and simplifying (34)

$$-\frac{\Delta P}{L} y = \tau - \tau_w \tag{35}$$

Therefore

$$\tau = \tau_w - \frac{\Delta P}{L} y \tag{36}$$

For yield Power law fluid in region I,

$$\tau = \tau_o + K\left(-\frac{dV}{dy}\right)^n \tag{37}$$

Substituting (36) into (37)

$$\tau_w - \frac{\Delta P}{L} y = \tau_o + K\left(-\frac{dV}{dy}\right)^n \tag{38}$$

Making $\frac{dV}{dy}$ the subject of the formula in (38)

$$\frac{dV}{dy} = -\frac{1}{K^{\frac{1}{n}}}\left(\tau_w - \frac{\Delta P}{L} y - \tau_o\right)^{\frac{1}{n}} \tag{39}$$

Integrating both sides of (28) with respect to y,

$$\int \frac{dV}{dy} dy = \int -\frac{1}{K^{\frac{1}{n}}}\left(\tau_w - \frac{\Delta P}{L} y - \tau_o\right)^{\frac{1}{n}} dy \tag{40}$$

Solving and applying the limits

$$\int_0^V dV = -\frac{1}{K^{\frac{1}{n}}}\int_0^y \left(\tau_w - \frac{\Delta P}{L}y - \tau_o\right)^{\frac{1}{n}} dy \tag{41}$$

Simplifying equation (41)

$$V = \frac{1}{K^{\frac{1}{n}}}\left(\frac{n}{n+1}\right)\left(\frac{L}{\Delta P}\right)\left(\tau_w - \frac{\Delta P}{L}y - \tau_o\right)^{\frac{n}{n+1}\ y}_{\ 0} \tag{42}$$

Since V is for region 1, V can be designated as V_1 and simplifying with the limits y and 0.

$$V_1 = \frac{1}{K^{\frac{1}{n}}}\left(\frac{n}{n+1}\right)\left(\frac{L}{\Delta P}\right)\left[\left(\tau_w - \frac{\Delta P}{L}y - \tau_o\right)^{\frac{n}{n+1}} - (\tau_w - \tau_o)^{\frac{n}{n+1}}\right] \tag{43}$$

Representing Equation (43) into dimensionless form by factorizing out $\frac{\Delta PH}{L}$ and also by dividing each term by $\frac{\Delta PH}{L}$.

$$\frac{V_1}{V_P} = \frac{1}{K^{\frac{1}{n}}}\left(\frac{n}{n+1}\right)\frac{1}{V_P}\left(\frac{L}{\Delta P}\right)\left(\frac{\Delta PH}{L}\right)^{\frac{n}{n+1}}\left[\left(\frac{\tau_w}{\frac{\Delta PH}{L}} - \frac{\tau_o}{\frac{\Delta PH}{L}} - \frac{\frac{\Delta P}{L}y}{\frac{\Delta PH}{L}}\right)^{\frac{n}{n+1}} - \left(\frac{\tau_w}{\frac{\Delta PH}{L}} - \frac{\tau_o}{\frac{\Delta PH}{L}}\right)^{\frac{n}{n+1}}\right] \tag{44}$$

Which is:

$$\frac{V_1}{V_P} = \frac{1}{K^{\frac{1}{n}}}\left(\frac{n}{n+1}\right)\frac{1}{V_P}\left(\frac{L}{\Delta P}\right)\left(\frac{\Delta PH}{L}\right)^{\frac{n}{n+1}}\left[\left(\frac{\tau_w - \tau_o}{\frac{\Delta PH}{L}} - \frac{y}{H}\right)^{\frac{n}{n+1}} - \left(\frac{\tau_w - \tau_o}{\frac{\Delta PH}{L}}\right)^{\frac{n}{n+1}}\right] \quad (45)$$

Simplifying:

$$\frac{V_1}{V_P} = \left(\frac{\Delta PH}{LK}\right)^{\frac{1}{n}}\left(\frac{n}{n+1}\right)\left(\frac{H}{V_p}\right)\left[\left(\frac{\tau_w - \tau_o}{\frac{\Delta PH}{L}} - \frac{y}{H}\right)^{\frac{n}{n+1}} - \left(\frac{\tau_w - \tau_o}{\frac{\Delta PH}{L}}\right)^{\frac{n}{n+1}}\right] \quad (46)$$

Applying boundary conditions

$$\frac{dV}{dy} = 0, at\ y = y_1$$

Applying condition above to equation (38)

$$\tau_w - \frac{\Delta P}{L}y = \tau_o + K\left(-\frac{dV}{dy}\right)^n$$

Therefore

$$\tau_w - \tau_o = K(-0)^n + \frac{\Delta P}{L}y_1 \quad (47)$$

Simplifying

$$\tau_w - \tau_o = \frac{\Delta P}{L}y_1 \quad (48)$$

Substituting (48) into (46), and simplifying:

$$\frac{V_1}{V_P} = \left(\frac{\Delta PH}{LK}\right)^{\frac{1}{n}}\left(\frac{n}{n+1}\right)\left(\frac{H}{V_p}\right)\left[\left(\frac{\frac{\Delta P}{L}y_1}{\frac{\Delta PH}{L}} - \frac{y}{H}\right)^{\frac{n}{n+1}} - \left(\frac{\frac{\Delta P}{L}y_1}{\frac{\Delta PH}{L}}\right)^{\frac{n}{n+1}}\right] \tag{49}$$

Therefore,

$$\frac{V_1}{V_P} = \left(\frac{\Delta PH}{LK}\right)^{\frac{1}{n}}\left(\frac{n}{n+1}\right)\left(\frac{H}{V_p}\right)\left[\left(\frac{y_1}{H} - \frac{y}{H}\right)^{\frac{n}{n+1}} - \left(\frac{y_1}{H}\right)^{\frac{n}{n+1}}\right] \tag{50}$$

Defining the following dimensionless parameters below:

$$\frac{V_1}{V_P} = \widetilde{V_1} \tag{51}$$

$$\frac{y_1}{H} = \widetilde{y_1} \tag{52}$$

$$\frac{y}{H} = \tilde{y} \tag{53}$$

$$\frac{n}{n+1} = b \tag{54}$$

$$\mathbf{P} = \left(\frac{n}{n+1}\right)\left(\frac{H}{V_p}\right)\left(\frac{\Delta PH}{LK}\right)^{\frac{1}{n}} \tag{55}$$

Applying all these dimensionless variables into (50), it becomes:

$$\widetilde{V_1} = \mathbf{P}[(\widetilde{y_1} - \tilde{y})^b - (\widetilde{y_1})^b] \tag{56}$$

Hence Equation (56) represents the dimensionless velocity profile for the yield power law fluid for region 1.

3.2.4 Velocity Profile Development for Region III, $y_2 \leq y \leq H$

From figure 12 consider a fluid element being acted upon by the forces shown below.

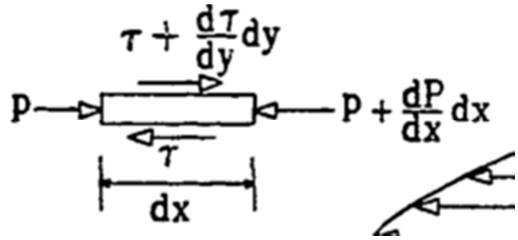

Figure 12: Pressure and Shear stress forces on yield power law fluid element in region III

$\overrightarrow{\sum F_x} = 0$

This then becomes

$$Pdy - \left(P + \frac{dP}{dx}dx\right)dy + \left(\tau + \frac{d\tau}{dy}dy\right)dx - \tau dx = 0 \qquad (57)$$

$$-\frac{dP}{dx}dxdy + \frac{d\tau}{dy}dydx = 0 \qquad (58)$$

Divide both sides of equation (58) by $dxdy$

$$\frac{dP}{dx} = \frac{d\tau}{dy} \tag{59}$$

Integrating both sides of equation (59) with respect to y

$$\int_{y_2}^{y} \frac{dP}{dx} dy = \int_{\tau_o}^{\tau} \frac{d\tau}{dy} dy \tag{60}$$

Letting$\frac{dP}{dx} = \frac{\Delta P}{L}$, and simplifying (60)

$$\frac{\Delta P}{L}(y - y_2) = (\tau - \tau_o) \tag{61}$$

So

$$\tau = \tau_o + \frac{\Delta P}{L}(y - y_2) \tag{62}$$

Note formula for Yield Power Law for region (III) is given by (63)

$$\tau = \tau_o + K\left(\frac{dV}{dy}\right)^n \tag{63}$$

Substituting (63) into Equation (62)

$$\tau_o + K\left(\frac{dV}{dy}\right)^n = \tau_o + \frac{\Delta P}{L}(y - y_2) \tag{64}$$

Simplifying and integrating (64), for velocity in region III:

$$\int_{V_3}^{V_p} dV = \int_{y}^{H} \left(\frac{\Delta P}{KL}\right)^{\frac{1}{n}} (y - y_2)^{\frac{1}{n}} dy \quad (65)$$

$$V_p - V_3 = \left(\frac{\Delta P}{KL}\right)^{\frac{1}{n}} \left(\frac{n}{n+1}\right) (y - y_2)^{\frac{n}{n+1}}{}_{y}^{H} \quad (66)$$

Substituting the limits:

$$V_p - V_3 = \left(\frac{\Delta P}{KL}\right)^{\frac{1}{n}} \left(\frac{n}{n+1}\right) \left[(H - y_2)^{\frac{n}{n+1}} - (y - y_2)^{\frac{n}{n+1}}\right] \quad (67)$$

Factorize out H from each term in the square bracket, and also divide both sides of equation withV_P. From above

$$1 - \frac{V_3}{V_p} = \left(\frac{\Delta PH}{KL}\right)^{\frac{1}{n}} \left(\frac{H}{V_p}\right) \left(\frac{n}{n+1}\right) \left[\left(1 - \frac{y_2}{H}\right)^{\frac{n}{n+1}} - \left(\frac{y}{H} - \frac{y_2}{H}\right)^{\frac{n}{n+1}}\right] \quad (68)$$

Also by definition already stated above:

$$\frac{V_3}{V_P} = \widetilde{V_3} \quad (69)$$

$$\frac{y_2}{H} = \widetilde{y_2} \quad (70)$$

$$\frac{y}{H} = \tilde{y} \quad (71)$$

$$\frac{n}{n+1} = b \quad (72)$$

$$\mathbf{P} = \left(\frac{n}{n+1}\right) \left(\frac{H}{V_p}\right) \left(\frac{\Delta PH}{LK}\right)^{\frac{1}{n}} \quad (73)$$

Applying the dimensionless variables to Equation (51), hence the dimensionless velocity profile for region III becomes:

$$1 - \widetilde{V_3} = \mathbf{P}[(1 - \widetilde{y_2})^b - (\tilde{y} - \widetilde{y_2})^b] \tag{74}$$

Rearranging the equation just above:

$$\widetilde{V_3} = 1 - \mathbf{P}[(1 - \widetilde{y_2})^b - (\tilde{y} - \widetilde{y_2})^b] \tag{75}$$

Note:

The equations for velocity profiles in the sheared region of the yield Power law fluid, Equations (56) and (75) are similar to that of Power Law fluid equations (22) and (23) respectively, but in addition to these, the yield power law fluid has a plug region.

3.2.5 Velocity Profile Development for the Plug Region II, $\boldsymbol{y_1 \leq y \leq y_2}$

Finding the plug thickness and for plug region at $y = y_1$:

$$\frac{dP}{dx} = -\frac{d\tau}{dy} \tag{76}$$

Integrating both sides of equation (3.52) with respect to y, and letting $\frac{dP}{dx} = \frac{\Delta P}{L}$, and simplifying

$$\frac{dP}{dx}\int dy = -\int \frac{d\tau}{dy} dy \tag{77}$$

$$-\tau = \frac{\Delta P}{L} y + C_1 \tag{78}$$

Applying the boundary conditions, at $y = y_1$, $\tau = \tau_o$, therefore

$$-\tau_o = \frac{\Delta P}{L} y_1 + C_1 \tag{79}$$

Stating equation for plug region at $y = y_2$ in figure 10

$$\frac{dP}{dx} = \frac{d\tau}{dy} \tag{80}$$

Integrating both sides of equation w.r.t y and substituting $y = y_2$

$$\tau = \frac{\Delta P}{L} y + C_1 \tag{81}$$

Applying boundary conditions, at $y = y_2$, $\tau = \tau_o$

$$\tau_o = \frac{\Delta P}{L} y_2 + C_1 \tag{82}$$

Combining equations (79) and (82) results in:

$$2\tau_o = \frac{\Delta P}{L} (y_2 - y_1) \tag{83}$$

$$(y_2 - y_1) = \frac{2\tau_o}{\frac{\Delta P}{L}} \tag{84}$$

Writing this in dimensionless, dividing both sides of equation (84) with H

$$(\widetilde{y_2} - \widetilde{y_1}) = \frac{2\tau_o}{\frac{\Delta P H}{L}} = \phi \tag{85}$$

and

$$\widetilde{y_2} = \phi + \widetilde{y_1} \tag{86}$$

Recalling the velocity profiles for regions I and III, equations (56) and (75)

$$\widetilde{V_1} = \mathbf{P}[(\widetilde{y_1} - \tilde{y})^b - (\widetilde{y_1})^b] \tag{56}$$

$$\widetilde{V_3} = 1 - \mathbf{P}[(1 - \widetilde{y_2})^b - (\tilde{y} - \widetilde{y_2})^b] \tag{75}$$

At the plug flow, the velocity is uniform, therefore at $y = \widetilde{y_1}$, the value of $\widetilde{V_1}$ is equal to $\widetilde{V_3}$ at $y = \widetilde{y_2}$

Substituting for $\widetilde{V_1}\ at\ y = \widetilde{y_1}$ into equation (56)

$$\widetilde{V_1} = \mathbf{P}(\widetilde{y_1} - \widetilde{y_1})^b - \mathbf{P}(\widetilde{y_1})^b = -\mathbf{P}(\widetilde{y_1})^b = \widetilde{V_2} \tag{87}$$

Substituting for $\widetilde{V_3}\ at\ y = \widetilde{y_2}$ into equation (75)

$$\widetilde{V_3} = 1 - \mathbf{P}[(1 - \widetilde{y_2})^b - (\widetilde{y_2} - \widetilde{y_2})^b] \tag{88}$$

$$\widetilde{V_3} = 1 - \mathbf{P}(1 - \widetilde{y_2})^b \tag{89}$$

Substituting for $\widetilde{y_2}$ from equation (86) into (89).

$$\widetilde{V_3} = 1 - \mathbf{P}(1 - \widetilde{y_1} - \phi)^b \tag{90}$$

From the analysis of plug flow, $\widetilde{V_1} = \widetilde{V_3}$. Equating (87) and (90).

$$1 - \mathbf{P}(1 - \widetilde{y_1} - \phi)^b = -\mathbf{P}(\widetilde{y_1})^b \tag{91}$$

Rearranging

$$-\mathbf{P}(1-\widetilde{y_1}-\phi)^b+\mathbf{P}(\widetilde{y_1})^b+1=0 \tag{92}$$

Dividing (92) by – $\mathbf{P}$

$$(1-\widetilde{y_1}-\phi)^b-(\widetilde{y_1})^b-\frac{1}{\mathbf{P}}=0 \tag{93}$$

Substituting back ϕ from Equation (85)

$$\left(1-\widetilde{y_1}-\frac{2\tau_o}{\frac{\Delta PH}{L}}\right)^b-(\widetilde{y_1})^b-\frac{1}{\mathbf{P}}=0 \tag{94}$$

Equation (3.61) is the identity equation for Yield Power Law fluid as developed by Crespo and Ahmed (2010), and when $\tau_o=0$ it is equal to that developed by Chukwu and Blick (1989).

Re-writing the equation (94).

$$\left(1-\widetilde{y_1}-\frac{2\tau_o}{\Delta PH/L}\right)^b-(\widetilde{y_1})^b-\frac{1}{\left(\frac{n}{n+1}\right)\left(\frac{H}{V_p}\right)\left(\frac{\Delta PH}{LK}\right)^{1/n}}=0 \tag{95}$$

3.2.6 Development Of Equations for Dimensionless flow rate

The expression for the flow rate is given by:

$$q=w\int_0^H V dy \tag{96}$$

Recall from dimensionless variable definition:

$$V = \tilde{V} V_p \tag{97}$$

$$y = \tilde{y} H \tag{98}$$

Substituting equations (97) and (98) into (96)

$$q = w \int_0^H \tilde{V} V_p d\,(\tilde{y} H) \tag{99}$$

$$\frac{q}{w H V_p} = \tilde{q} = \int_0^1 \tilde{V} d\,\tilde{y} \tag{100}$$

Since the velocity profile is for three regions, the integration above will be done for the three velocities and the corresponding interval.

$$\tilde{q_t} = \int_0^{\widetilde{y_1}} \widetilde{V_1}\, d\tilde{y} + \int_{\tilde{y}_1}^{\widetilde{y_2}} \widetilde{V_2}\, d\tilde{y} + \int_{\tilde{y}_2}^1 \widetilde{V_3}\, d\tilde{y} \tag{101}$$

Solving the first integral, substituting the velocity profile:

$$\int_0^{\widetilde{y_1}} \widetilde{V_1}\, d\tilde{y} = \int_0^{\widetilde{y_1}} \mathbf{P}[(\widetilde{y_1} - \tilde{y})^b - (\widetilde{y_1})^b]\; d\tilde{y} = -\ \mathbf{P}\,(\widetilde{y_1})^{b+1} \left(\frac{b}{b+1}\right) \tag{102}$$

And for the second:

$$\int_{\tilde{y}_1}^{\widetilde{y_2}} \widetilde{V_2}\, d\tilde{y} = \int_{\tilde{y}_1}^{\widetilde{y_2}} -\ \mathbf{P}\,(\widetilde{y_1})^b\, d\tilde{y} = \ -\ \mathbf{P}(\widetilde{y_2} - \widetilde{y_1})\,(\widetilde{y_1})^b \tag{103}$$

Applying equation (85) to (103), the integral above becomes

$$\int_{\tilde{y}_1}^{\widetilde{y_2}} \widetilde{V_2}\, d\tilde{y} = -\ \mathbf{P}\phi\,(\widetilde{y_1})^b \tag{104}$$

And the third integral in equation (101)

$$\int_{\tilde{y}_2}^{1} \widetilde{V_3}\, d\tilde{y} = \int_{\tilde{y}_2}^{1} (1 - \mathbf{P}[(1 - \widetilde{y_2})^b - (\tilde{y} - \widetilde{y_2})^b])\, d\tilde{y} \tag{105}$$

Simplifying (3.80) results in:

$$= -[\mathbf{P}\,(1 - \widetilde{y_2})^b - 1][1 - \widetilde{y_2}] + \frac{\mathbf{P}}{b+1}(1 - \widetilde{y_2})^{b+1} \tag{106}$$

So in computing (101), by adding results from (102), (103) and (106)

$$\widetilde{q_t} = -\ \mathbf{P}\left(\frac{b}{b+1}\right)(\widetilde{y_1})^{b+1} - [\mathbf{P}\,(1 - \widetilde{y_2})^b - 1][1 - \widetilde{y_2}] + \frac{\mathbf{P}}{b+1}(1 - \widetilde{y_2})^{b+1} - \mathbf{P}\phi\,(\widetilde{y_1})^b \tag{107}$$

Substituting for $\widetilde{y_2}$ by applying (86) into (107)

$$\widetilde{q_t} = -\ \mathbf{P}\left(\frac{b}{b+1}\right)(\widetilde{y_1})^{b+1} - [\mathbf{P}\,(1 - \widetilde{y_1} - \phi)^b - 1][1 - \widetilde{y_1} - \phi] + \frac{\mathbf{P}}{b+1}(1 - \widetilde{y_1} - \phi)^{b+1} - \mathbf{P}\phi\,(\widetilde{y_1})^b \tag{108}$$

Note Equation (108) is now only in terms of the variable $\widetilde{y_1}$

Also dimensionless flow rate is given as:

$$\widetilde{q_t} = \frac{-q}{WHV_p} \tag{109}$$

For the well bore:

$$H = \frac{(d_h - d_p)}{2} \tag{110}$$

Slot width:

$$W = \frac{\pi}{2}\left(d_h - d_p\right) \tag{111}$$

For a closed-pipe condition, the fluid rate in annular geometry is equal to the rate at which the fluid is displaced:

$$q = (\pi/4) d_p^2 V_p \tag{112}$$

Substituting (110), (111) and (112) into (109)

$$\widetilde{q_t} = \frac{-1}{\left(\frac{d_h}{d_p}\right)^2 - 1} \tag{113}$$

These equations would then be applied in determining the surge and swab pressure profiles.

CHAPTER FOUR

APPLICATION OF CONFORMAL MAPPING TO ECCENTRIC ANNULUS

4.1 Introduction

In the preceding chapters, the phenomenon of eccentricity was looked at. The corresponding formulation which consists of a varying eccentric height was looked at. Also the slot model formulation for Yield Power law fluids was also looked at, and it was also related to power law fluids in concentric annulus.

This study looks at providing a surge and swab profile for Yield Power Law fluids in Eccentric Annulus. But currently since formulation has been done for yield power law fluids in concentric annulus, then it would be of interest to find a connection between the concentric and eccentric annulus.

The mathematical tool that would be used to solve this problem is Conformal Mapping. **Conformal mapping** is a concept mostly used in physical applications involving fluid movement, heat conduction, aerodynamics, and electrostatic potential, but as a mathematical concept it can also be applied to any field where surface deformations are present. (Perez, 2011)

The concept here is that the geometry involved, which is the eccentric annulus, can be mapped to a much simpler geometry which is the concentric annulus, which has already been presented in previous chapters.

If the physical problem can be represented by complex functions but the geometric structure becomes inconvenient then by an appropriate mapping it can be transferred to a problem with much more convenient geometry. Conformal mappings are invaluable for solving problems in engineering and physics that can be expressed in terms of functions of a complex variable, but exhibit inconvenient geometries. By choosing an appropriate mapping, the analyst can transform the inconvenient geometry into a much more convenient one. (Suman 2008)

4.2 Mapping of Eccentric Annulus Using Bilinear Function

The eccentric annulus will be mapped using the bilinear transformation:

$$z = \frac{aw + b}{cw + d} \tag{114}$$

Where a, b, c, d are constants. Z is the plane, given by $z = x + iy \; or \; z = re^{i\theta}$ while w is the plane given by $= u + iv \; or \; w = \rho e^{i\theta}$.

Solving equation (114) for w:

$$w = \frac{-dz + b}{cz - a} \tag{115}$$

The bilinear transformation has a remarkable property that circles map to as circles. (Chen, Tsai, and Liu 2008)

The equation of any circle in the z plane is known to be in the form:

$$A(x^2 + y^2) + Bx + Cy + D = 0 \tag{116}$$

For the eccentric annulus, the bilinear transformation that will be used is in the form:

$$z = \frac{w}{1 - aw} \tag{117}$$

a, is a real positive constant.

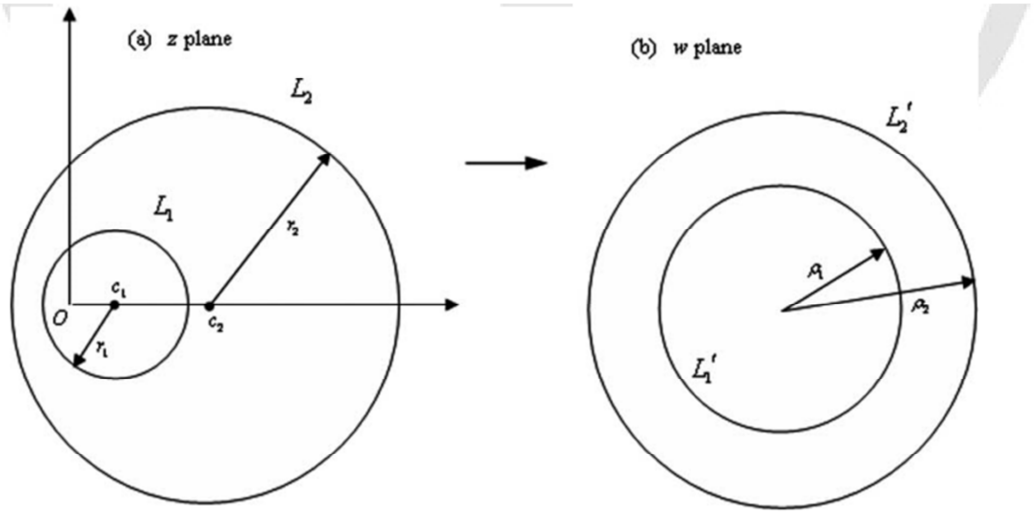

Figure 13: Mapping from the eccentric region to the concentric region (Chen, Tsai, and Liu 2008)

In figure 13 above, in the z plane the origin of the smaller circle with radius, r_1, is given as $(c_1,0)$. While the origin of the bigger circle with radius, r_2, is given as $(c_2,0)$. The circles map correspondingly into circles of new radii, ρ_1 and ρ_2 respectively which is now concentric. It can be shown that the centers and radii in the z plane for both circles are given as:

$$c_1 = \frac{a\rho_1^2}{1 - a^2\rho_1^2} \tag{118}$$

$$c_2 = \frac{a\rho_2^2}{1 - a^2\rho_2^2} \tag{119}$$

$$r_1 = \frac{\rho_1}{1 - a^2\rho_1^2} \tag{120}$$

and

$$r_2 = \frac{a\rho_2}{1 - a^2\rho_2^2} \tag{121}$$

respectively.

The distance between the centers c_1 and c_2, is given by the offset distance e.

$$e = c_2 - c_1 = \frac{a\rho_2^2}{1 - a^2\rho_2^2} - \frac{a\rho_1^2}{1 - a^2\rho_1^2} \tag{122}$$

From equations (120) and (121), and solving for the new radii.

From (4.95)

$$r_1 - a^2\rho_1^2 r_1 = \rho_1 \tag{123}$$

Rearranging:

$$a^2\rho_1^2 r_1 + \rho_1 - r_1 = 0 \tag{124}$$

Solving the quadratic equation forρ_1, using quadratic formula:

$$\rho_1 = \frac{-1 \pm \sqrt{1 - 4a^2 r_1(-r_1)}}{2 r_1 a^2} \tag{125}$$

Taking only the positive square root as a real solution.

$$\rho_1 = \frac{\sqrt{1 + 4a^2 r_1^2} - 1}{2 r_1 a^2} \tag{126}$$

By inference also the second radii is:

$$\rho_2 = \frac{\sqrt{1 + 4a^2 r_2^2} - 1}{2 r_2 a^2} \tag{127}$$

Also solving for a

$$a = \frac{e}{\sqrt{(r_1^2 - r_2^2)^2 - 2e^2(r_1^2 + r_2^2) + e^4}} \tag{128}$$

(culled from Chen, Tsai, and Liu 2008)

All the parameters for the Eccentric annulus have been defined into a new concentric format .

And recall that the slot height for a concentric annulus is constant.

Recall from equation (9) that $e = c\varepsilon$ and so substituting into equation (128)

$$a = \frac{c\varepsilon}{\sqrt{(r_1^2 - r_2^2)^2 - 2c^2\varepsilon^2(r_1^2 + r_2^2) + c^4\varepsilon^4}} \tag{129}$$

Equation (129) shows that the value, a, is function of radii r_1, r_2, clearance, c, and most essentially the eccentricity ratio, ε.

Recall that the clearance, c is given by equation (7). Substituting for $r_o = r_2$ and $r_i = r_1$. Therefore:

$$c = (r_2 - r_1) \tag{130}$$

Recall in the mapped eccentric annulus to concentric, the concentric height, H, is now given by:

$$H = \rho_2 - \rho_1 \tag{131}$$

And this can be evaluated using appropriately equations (101) and (102).

The new formula for H, (4.106), is used for the procedure for the concentric annulus. Recall (113)

$$\widetilde{q_t} = \frac{-1}{\left(\frac{d_h}{d_p}\right)^2 - 1}$$

Making inference of this equation (113) to the new configuration of radii, ρ_2, ρ_1, taking note that for any two concentric circles the ratio of diameters is the same as the ratio of corresponding radii. Therefore:

$$\widetilde{q_t} = \frac{-1}{\left(\frac{\rho_2}{\rho_1}\right)^2 - 1} \tag{132}$$

Also from (132):

$$\left(\frac{\rho_1}{\rho_2}\right) = \left(1 - \frac{1}{\widetilde{q_t}}\right)^{-0.5} \tag{133}$$

CHAPTER FIVE

APPLICATION OF YIELD POWER LAW SLOT MODEL TO EQUIVALENT CONCENTRIC ANNULUS FROM MAPPED ECCENTRIC ANNULUS

5.1 PROCEDURE:

The following procedures are followed to determine surge and swab pressures:

1) Given for a particular **eccentricity ratio or fraction, ε,** the clearance, c, is determined from the hole and tubular geometry given by equation (7) and the offset distance, e, is then calculated from equation (8)
2) The value of the clearance known already, then value, a, is calculated from equation (128) and this is the real positive value used for the mapping transformation.
3) The values ρ_1, ρ_2, and H are computed respectively from Equations (126), (127), and (131) respectively.
4) The value of b using equation (54) is computed for the specific yield power law drilling fluid model.
5) The value of $\widetilde{y_1}$ is gotten by solving equations (94) or (95). It is solved by using secant method, and it is solved for various $\left(\frac{\Delta P}{\Delta L}\right)$ and the specificV_p, with its corresponding dimensionless Pressure, P and ϕ evaluated for each case.
6) The corresponding values for dimensionless flow rate, $\widetilde{q_t}$, are determined using equation (108)
7) Characteristic plots of $(\Delta P/\Delta L)$ versus $\widetilde{q_t}$ are prepared for specific value ofV_p.

8) From equation (133) the value of$\widetilde{q_t}$, is computed and used as an input into the characteristic curves, and the corresponding value of $(\Delta P/\Delta L)$ is obtained for the particularV_p.

9) Then the surge or swab pressure is then calculated as:

$$\Delta P_s = (\Delta P/\Delta L) * L \qquad (134)$$

Note the above procedures from 1 to 9, are for a particular eccentricity ratio, ε. The procedures can be repeated for a different eccentricity ratio.

5.2 APPLICATION OF THE PROCEDURE TO DETERMINING SURGE AND SWAB PRESSURE

PROBLEM 1.

In a directional well, a 7-inch casing string is being lowered at a velocity of 0.5 ft/sec into a 10-inch hole. The diameter of casing collars is 8.5 inches and the mud in the hole has a flow behavior index, n equal to 0.8 with a consistency index, K equal to 300 eq. cp (0.0062658 lbf-sec^n/ft^2). Assume the fluid is a yield power law fluid yield stress of 10 lbf/100ft^2. What would be the surge pressure when running down hole?

SOLUTION:

i) The eccentricity ratio, $\varepsilon = \frac{10-8.5}{10-7} = 0.50$

ii) n = 0.80

$$b = \frac{n}{n+1}$$

$$b = \frac{0.8}{0.8+1} = 0.4444$$

iii) Given $\tau_0 = 10$ lbf/100 ft^2, K = 0.0062658 lbf-sec^n/ft^2 = 0.62658 lbf-sec^n/100ft^2, Vp = 0.5 fps.

iv) d_2 = 10.0 inch, d_1 = 7.0 inch

Therefore

$$r_2 = \frac{10}{2} = 5.0''$$

$$r_1 = \frac{7}{2} = 3.5''$$

v) The annular clearance, C is given by (130):

$$c = r_2 - r_1 = 5.0'' - 3.5'' = 1.5\ ''$$

vi) Then the offset distance, e, is computed by using equation (9)

$$e = c\varepsilon = 1.5(0.5) = 0.75$$

vii) Then the application of conformal mapping hence to solve for the new radii, from equations (128), (127) and (126)

$$a = \frac{0.75}{\sqrt{(5^2 - 3.5^2)^2 - 2(0.75^2)(5^2 + 3.5^2) + 0.75^4}} = 0.068190\ in^{-1}$$

$$\rho_2 = \frac{\sqrt{1 + 4(0.068190^2)(5^2)} - 1}{2(5)(0.068190^2)} = 4.5241\ in$$

$$\rho_1 = \frac{\sqrt{1+4(0.068190^2)(3.5^2)}-1}{2(3.5)(0.068190^2)} = 3.3206\ in$$

So, the eccentric circle is now concentric, with radii, $\rho_1 = 3.3206\ in$ and$\rho_2 = 4.5241\ in$. So, with the concentric geometry it is easier to solve the original eccentric geometry.

viii) Therefore concentric height, from equation (131)

$$\text{H} = \rho_2 - \rho_1 = 1.2035\ in$$

A table is then produced for different combinations of, $(\Delta P/L)$,ϕ, Vp, and$\boldsymbol{P}$. From the various combinations, the dimensionless length was solved using Matlab Program secant method and with simulation. Also the dimensionless flow rate was evaluated.

ix) A graph of dimensionless pressure versus dimensionless flow rate and dimensionless radii was plotted and a graph of Pressure gradient versus dimensionless flow rate was plotted as well.

x) With the graphs already plotted, the specific dimensionless flow rate is calculated using Equation (132)

$$\widetilde{q_t} = \frac{-1}{\left(\frac{\rho_2}{\rho_1}\right)^2 - 1} = \frac{-1}{\left(\frac{4.5241}{3.3206}\right)^2 - 1} = -1.1679$$

With this value, the dimensionless pressure can be obtained from the chart of dimensionless pressure against dimensionless flow rate or evaluated using the chart equation. (Figure 14)

xi) Therefore reading from chart, or using the equation: (Figure 14)

P = 0.0167$\widetilde{q_t}^3$ + 0.4145$\widetilde{q_t}^2$ - 0.0895$\widetilde{q_t}$+ 6.9221, Substituting $\widetilde{q_t} = -1.1679$

$$P = 0.0167(-1.1679^3) + 0.4145(-1.1679^2) - 0.0895(-1.1679) + 6.922$$

$$P = 7.5654$$

This can also be read from the graph of Dimensionless Pressure versus Dimensionless Flow rate.

xii) The surge pressure can then be calculated from equation (73).

$$\frac{\Delta P}{L} = \frac{P^n}{\left(\frac{n}{n+1}\right)^n \left(\frac{H}{V_p}\right)^n \left(\frac{H}{K}\right)} \qquad (135)$$

$$\frac{\Delta P}{L} = \frac{7.5654^{0.8}}{\left(\frac{0.8}{0.8+1}\right)^{0.8} \left(\frac{1.2036}{12 \times 0.5}\right)^{0.8} \left(\frac{1.2036}{12 \times 0.0062658}\right)} = 2.1808\ psf/ft$$

Appropriately converting the value above by dividing by 144 sq inches, therefore

$$\frac{\Delta P}{L} = 0.01514\ psi/ft$$

And with the value of the length of the drill string or tubular goods, the value of the surge or swab can then be evaluated.

xiii) Also this can be checked with from the graph of pressure surge versus dimensionless flow rate. The fitted equation is given as:

$\frac{\Delta P}{L} = 0.00003\widetilde{q_t}3 + 0.0006\widetilde{q_t}2 - 0.0004\widetilde{q_t} + 0.0139$, and when $\widetilde{q_t} = -1.1679$

Substituting,

$$\frac{\Delta P}{L} = 0.00003(-1.1679^3) + 0.0006(-1.1679^2) - 0.0004(-1.1679) + 0.0139$$

$$\frac{\Delta P}{L} = 0.01514\ psi/ft$$

This value can also be read from the graph. The computed value is also exactly close to that computed in step (xii).

ε	n	b	$\tau_o(lbf/100ft^2)$	$k(lbf.s^n/100ft^2)$	$d_2(in)$	$d_1(in)$	$r_2(in)$	$r_1(in)$
0.50	0.80	0.4444	10.0000	0.626580	10.0000	7.0000	5.000	3.500

$c(in)$	$e(in)$	$a(in^{-1})$	$\rho_2(in)$	$\rho_1(in)$	$H(in)$
1.500	0.750	0.06819	4.5241	3.3206	1.2036

Table 2: Procedure for computation of different hole parameters given the input parameters.

$\Delta P/L$ (Psi/ft)	V_p (fps)	ϕ	**P**
0.015	0.50	0.9232	7.4749
0.016		0.8655	8.1030
0.017		0.8146	8.7409
0.018		0.7693	9.3883
0.019		0.7288	10.0447
0.020		0.6924	10.7098
0.021		0.6594	11.3833
0.022		0.6294	12.0649
0.023		0.6021	12.7542
0.024		0.5770	13.4511
0.025		0.5539	14.1553
0.026		0.5326	14.8666
0.027		0.5129	15.5847
0.028		0.4946	16.3095
0.029		0.4775	17.0409
0.030		0.4616	17.7785
0.031		0.4467	18.5224
0.032		0.4327	19.2722
0.033		0.4196	20.0280
0.034		0.4073	20.7894
0.035		0.3956	21.5565
0.036		0.3847	22.3292
0.037		0.3743	23.1071
0.038		0.3644	23.8904
0.039		0.3551	24.6789
0.040		0.3462	25.4724

Table3: Showing various pressure gradient with corresponding with dimensionless parameter $\boldsymbol{\phi}$, and dimensionless pressure P, for particular tripping speed of Vp = 0.5 fps.

$\widetilde{y_1}$	$\widetilde{q_t}$	$\left(\frac{\rho_1}{\rho_2}\right)$
0.01538	-1.0641	0.7180
0.03702	-1.6307	0.7873
0.05907	-2.0793	0.8217
0.07957	-2.4569	0.8430
0.09895	-2.7994	0.8584
0.11695	-3.1155	0.8701
0.13354	-3.4119	0.8794
0.14893	-3.6944	0.8871
0.16314	-3.9654	0.8936
0.17651	-4.2295	0.8993
0.18863	-4.4835	0.9042
0.20005	-4.7332	0.9086
0.21069	-4.9782	0.9125
0.22063	-5.2192	0.9161
0.22992	-5.4569	0.9193
0.23872	-5.6925	0.9223
0.24692	-5.9251	0.9250
0.25466	-6.1561	0.9275
0.26196	-6.3854	0.9298
0.26883	-6.6130	0.9320
0.27534	-6.8396	0.9340
0.28151	-7.0653	0.9360
0.28736	-7.2901	0.9377
0.29291	-7.5142	0.9394
0.29818	-7.7377	0.9410
0.30300	-7.9591	0.9425

Table 4: Showing solved corresponding dimensionless distance solved using Iterative simulation technique and computed dimensionless flow rate and dimensionless radii respectively.

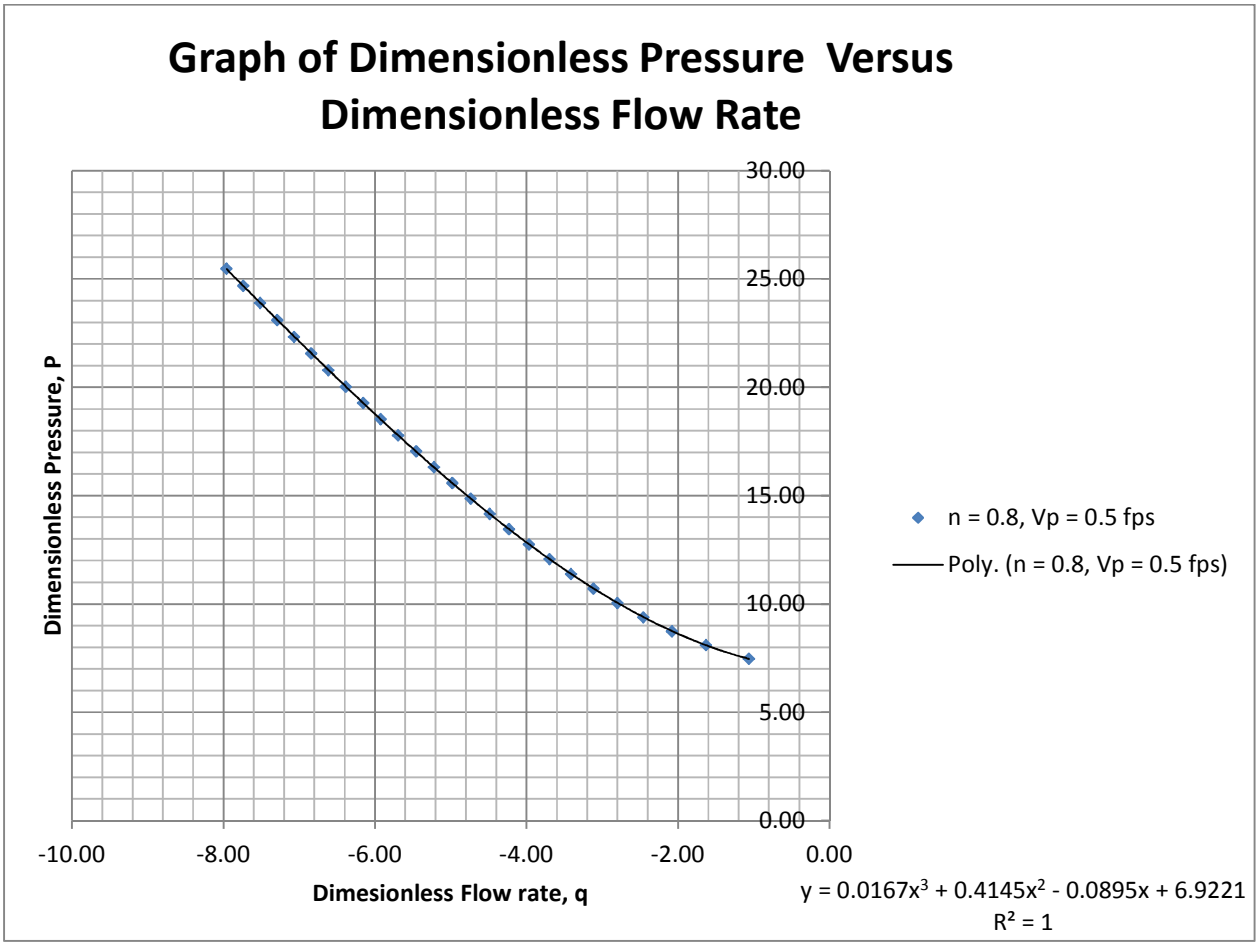

Figure 14: Graph of Dimensionless Pressure Versus Dimensionless Flow Rate (For ε = 0.5, shear stress $\tau_0 = 10$ lbf/100 ft^2, flow behavior index n =0.80, consistency index K = 0.0062658 lbf-sec^n/ft^2 = 0.62658 lbf-sec^n/100ft^2)

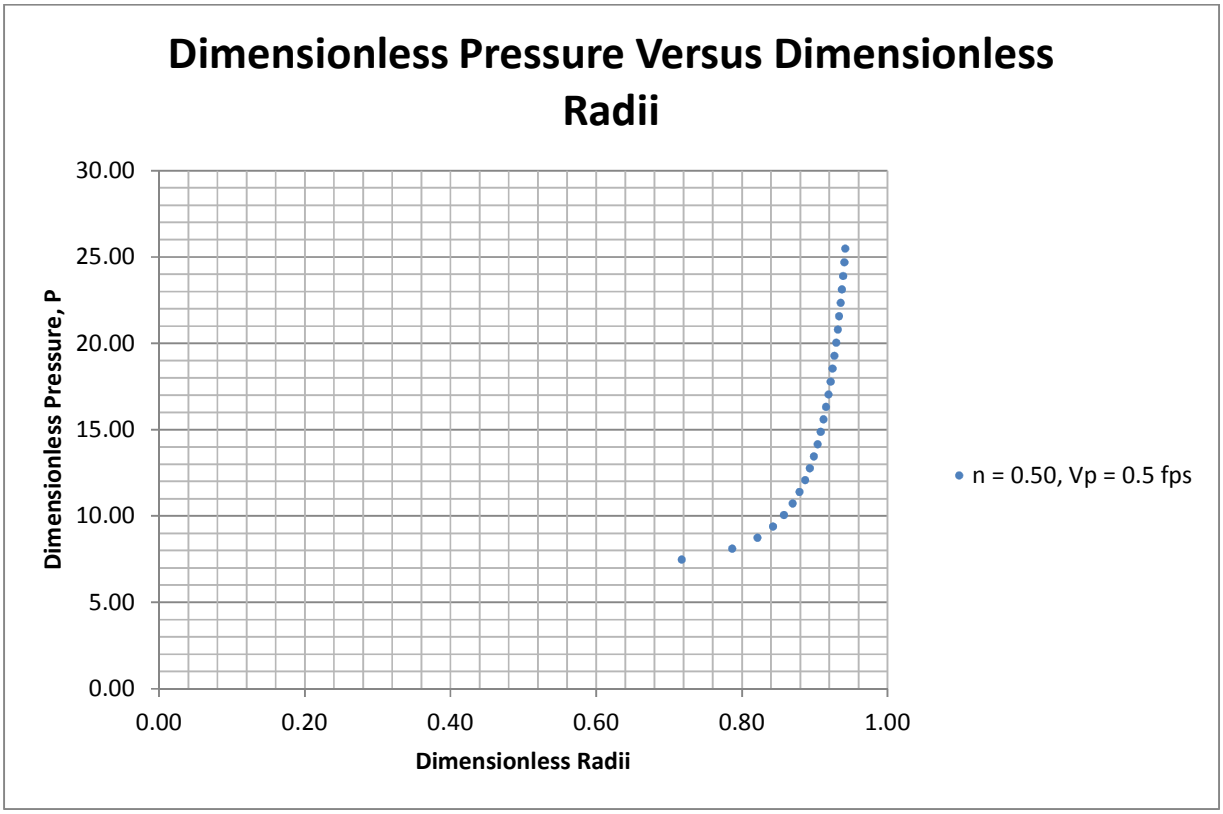

Figure 15: Graph of Dimensionless Pressure Versus Dimensionless Radii (For ε = 0.5, shear stress $\tau_0 = 10$ lbf/100 ft^2, flow behavior index n =0.80, consistency index K = 0.0062658 lbf-sec^n/ft^2 = 0.62658 lbf-sec^n/100ft^2)

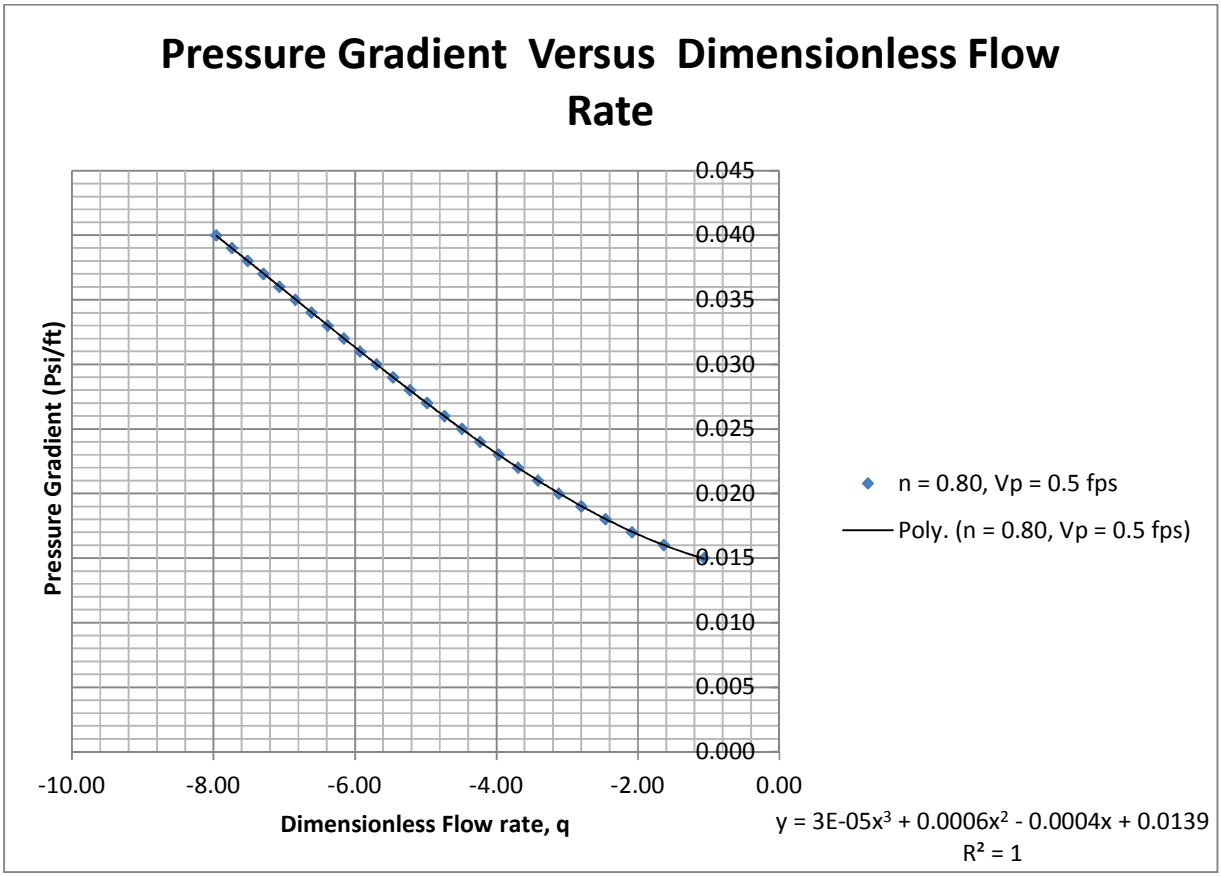

Figure 16: Graph of Dimensionless Pressure Versus Dimensionless Radii (For ε = 0.5, shear stress τ_0 = 10 lbf/100 ft^2, flow behavior index n =0.80, consistency index K = 0.0062658 lbf-sec^n/ft^2 = 0.62658 lbf-sec^n/100ft^2)

PROBLEM 2:

In a directional well, a 7-inch casing string is being lowered at a velocity of 0.5 ft/sec into a 10-inch hole. If the eccentricity ratio is 0.8, and the mud in the hole has a flow behavior index, n equal to 0.8 with a consistency index, K equal to 300 eq. cp (0.0062658 lbf-sec^n/ft^2). Assume the fluid is a yield power law fluid yield stress of 10 lbf/100ft^2. What would be the surge pressure when running down hole?

SOLUTION:

Now the problem is resolved maintaining the same parameters, except that the eccentricity ratio is now increased to 0.80. The effect now is to observe the value of the surge pressure, if it increases or reduces?

SOLUTION:

i) ε = 0.80

ii) n = 0.80

Therefore from (3.39d)

$$b = \frac{n}{n+1}$$

$$b = \frac{0.8}{0.8+1} = 0.4444$$

iii) Given $\tau_0 = 10$ lbf/100 ft^2, K = 0.0062658 lbf-sec^n/ft^2 = 0.62658 lbf-sec^n/100ft^2, Vp = 0.5 fps.

iv) d_2 = 10.0 inch, d_1 = 7.0 inch

Therefore

$$r_2 = \frac{10}{2} = 5.0\,''$$

$$r_1 = \frac{7}{2} = 3.5\,''$$

v) The annular clearance, C is given by (130):

$$c = r_2 - r_1 = 5.0 - 3.5 = 1.5\,''$$

vi) Then the offset distance, e, is computed by equation (9)

$$e = c\varepsilon = 1.5(0.8) = 1.20\,"$$

vii) Then the application of conformal mapping hence to solve for the new radii, from Equations (128), (127), (126)

$$a = \frac{1.2}{\sqrt{(5^2 - 3.5^2)^2 - 2(1.2^2)(5^2 + 3.5^2) + 1.2^4}} = 0.158445\ in^{-1}$$

$$\rho_2 = \frac{\sqrt{1 + 4(0.158445^2)(5^2)} - 1}{2(5)(0.158445^2)} = 3.47992\ in$$

$$\rho_1 = \frac{\sqrt{1 + 4(0.158445^2)(3.5^2)} - 1}{2(3.5)(0.158445^2)} = 2.80745\ in$$

So, the eccentric circle is now concentric, with radii, $\rho_1 = 2.80745\ in$ and $\rho_2 = 3.47992\ in$. So, with the concentric geometry it is easier to solve than the original eccentric geometry.

viii) Therefore concentric height, by Equation (131)

$$\text{H} = \rho_2 - \rho_1 = 0.67247\ in$$

A table is then produced for different combinations of, $(\Delta P/L)$, ϕ, Vp, and $\boldsymbol{P}$. From the various combinations, the dimensionless length was solved using Matlab Program secant method and also with simulation. Also the dimensionless flow rate was evaluated.

ix) A graph of dimensionless pressure versus dimensionless flow rate and dimensionless radii was then plotted and also a graph of Pressure gradient versus dimensionless flow rate was plotted as well.

x) With the graphs already plotted, the specific dimensionless flow rate is calculated using Equation (132)

$$\widetilde{q_t} = \frac{-1}{\left(\frac{\rho_2}{\rho_1}\right)^2 - 1} = \frac{-1}{\left(\frac{3.47992}{2.80745}\right)^2 - 1} = -1.8642$$

With this value, the dimensionless pressure can be read from the chart of dimensionless pressure against dimensionless flow rate or evaluated using the chart equation. (Figure 17)

xi) Therefore reading from chart, or using the equation: y = $0.0528x^3 + 0.6942x^2 - 0.4496x + 4.0196$ (Figure 17)

$P = 0.0528\widetilde{q_t}^3 + 0.6942\widetilde{q_t}^2 - 0.4496\widetilde{q_t} + 4.0196$ Substituting $\widetilde{q_t} = -1.8642$

$P = 0.0528(-1.8642^3) + 0.6942(-1.8642^2) - 0.4496(-1.8642) + 4.0196$

$P = 6.9282$

This can also be read from the graph.

xii) The surge pressure can then be calculated from equation (73).

$$\frac{\Delta P}{L} = \frac{P^n}{\left(\frac{n}{n+1}\right)^n \left(\frac{H}{V_p}\right)^n \left(\frac{H}{K}\right)} \qquad (135)$$

$$\frac{\Delta P}{L} = \frac{6.9282^{0.8}}{\left(\frac{0.8}{0.8+1}\right)^{0.8} \left(\frac{0.6724}{12 \times 0.5}\right)^{0.8} \left(\frac{0.6724}{12 \times 0.0062658}\right)} = 5.7968\ psf/ft$$

Appropriately converting the value above by dividing by 144 sq inches, therefore

$\frac{\Delta P}{L} = 0.04025\ psi/ft$

And with the value of the length of the drill string or tubular goods, the value of the surge or swab can then be evaluated. This value can also be read from the graph of pressure gradient versus dimensionless flow rate.

xiii) Also this can be checked with from the graph of pressure surge versus dimensionless flow rate. The fitted equation is given as: (figure 19) $y = 0.0004x^3 + 0.0035x^2 - 0.0024x + 0.026$

$\frac{\Delta P}{L} = 0.0004\widetilde{q_t}^3 + 0.0035\widetilde{q_t}^2 - 0.0024\widetilde{q_t} + 0.026$, and when $\widetilde{q_t} = -1.8642$

Substituting,

$$\frac{\Delta P}{L} = 0.0004(-1.8642^3) + 0.0035(-1.8642^2) - 0.0024(-1.8642) + 0.026$$

$$\frac{\Delta P}{L} = 0.0400\ psi/ft$$

This value can also be read from the graph. The computed value is also quite close to that computed in step (xii).

ε	n	b	$\tau_o(lbf/100ft^2)$	$k(lbf.s^n/100ft^2)$	$d_2(in)$	$d_1(in)$	$r_2(in)$	$r_1(in)$
0.80	0.80	0.4444	10.0000	0.626580	10.0000	7.0000	5.000	3.500

$c(in)$	$e(in)$	$a(in^{-1})$	$\rho_2(in)$	$\rho_1(in)$	$H(in)$	$\tilde{q}_t$
1.500	1.200	0.15845	3.4799	2.8074	0.6724	-1.8642

Tables 5: showing procedure for computation of different parameters given the input parameters.

The table 5 above shows the different columns in an Excel Program, the columns for eccentricity ratio, hole diameter, tubular goods diameter, fluid behavior index, yield stress and consistency index. The other columns were computed using the appropriate formula.

$\Delta P/L$ (Psi/ft)	V_p (fps)	ϕ	**P**	
0.025	0.50	0.9914	3.8202	
0.026		0.9533	4.0121	
0.027		0.9180	4.2059	
0.028		0.8852	4.4015	
0.029		0.8547	4.5989	
0.030		0.8262	4.7980	
0.031		0.7995	4.9987	
0.032		0.7745	5.2011	
0.033		0.7511	5.4050	
0.034		0.7290	5.6105	
0.035		0.7081	5.8176	
0.036		0.6885	6.0261	
0.037		0.6699	6.2360	
0.038		0.6522	6.4474	
0.039		0.6355	6.6602	
0.040		0.6196	6.8743	
0.041		0.6045	7.0898	
0.042		0.5901	7.3066	
0.043		0.5764	7.5247	
0.044		0.5633	7.7441	
0.045		0.5508	7.9647	
0.046		0.5388	8.1866	
0.047		0.5273	8.4096	
0.048		0.5164	8.6339	
0.049		0.5058	8.8593	
0.050		0.4957	9.0859	

Table 6: Showing various pressure gradient with corresponding with dimensionless parameter $\boldsymbol{\phi}$, and dimensionless pressure P, for particular tripping speed of Vp = 0.5 fps.

$\widetilde{y_1}$	$\widetilde{q_t}$	$\left(\frac{\rho_1}{\rho_2}\right)$	
	0.007378	#NUM!	
0.00002	0.0035	#NUM!	
0.00387	-0.2818	0.4688	
0.01154	-0.4861	0.5719	
0.02090	-0.6550	0.6291	
0.03080	-0.7997	0.6666	
0.04131	-0.9341	0.6950	
0.05146	-1.0536	0.7163	
0.06169	-1.1674	0.7339	
0.07175	-1.2753	0.7487	
0.08164	-1.3788	0.7613	
0.09108	-1.4768	0.7722	
0.10030	-1.5721	0.7818	
0.10926	-1.6647	0.7904	
0.11788	-1.7546	0.7981	
0.12620	-1.8423	0.8051	
0.13423	-1.9281	0.8115	
0.14202	-2.0126	0.8174	
0.14950	-2.0954	0.8228	
0.15628	-2.1743	0.8276	
0.16363	-2.2570	0.8324	
0.17025	-2.3358	0.8368	
0.17685	-2.4149	0.8409	
0.18277	-2.4906	0.8447	
0.18912	-2.5692	0.8484	
0.19498	-2.6455	0.8519	

Table 7: Showing solved corresponding dimensionless distance solved using Iterative simulation technique and corresponding computed dimensionless flow rate and dimensionless radii respectively

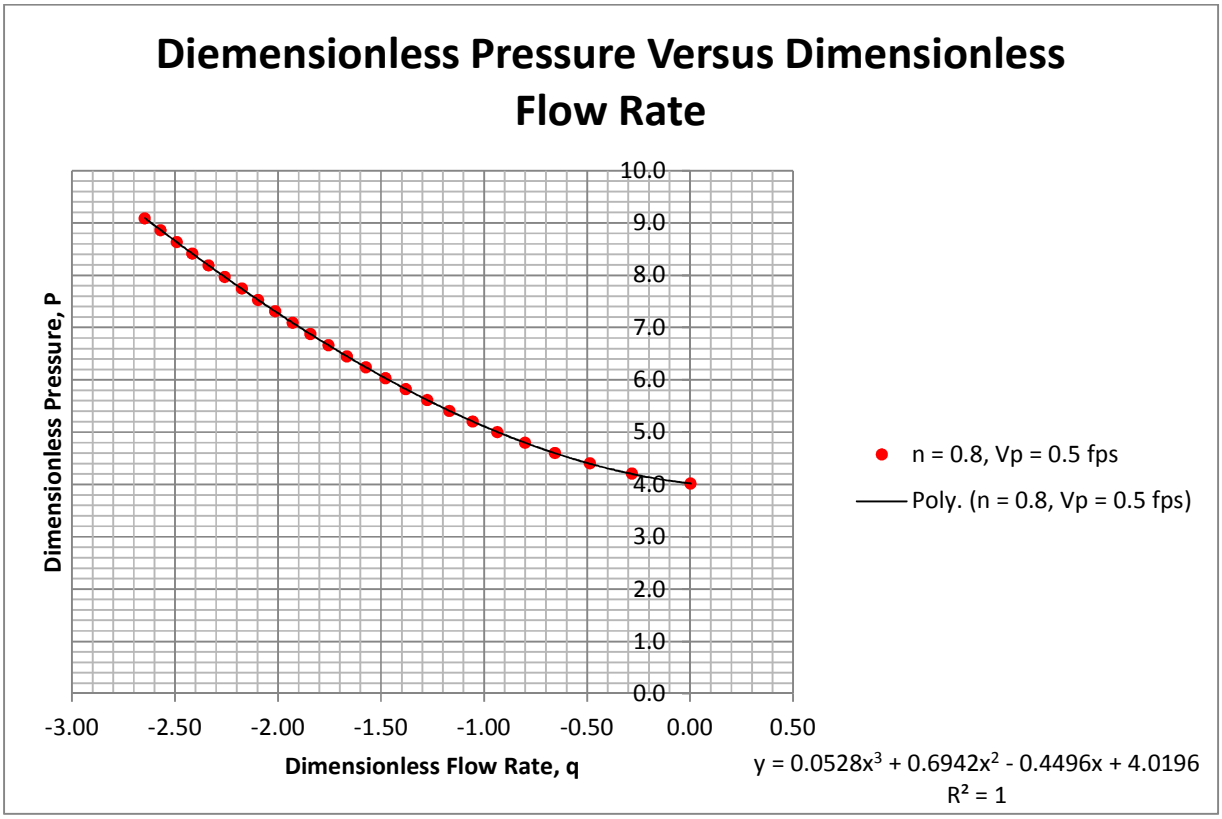

Figure 17: Graph of Dimensionless Pressure Versus Dimensionless Flow Rate, (For ε = 0.8,Shear stress τ_0 = 10 lbf/100 ft^2, flow behavior index n =0.80, consistency index K = 0.0062658 lbf-sec^n/ft^2 = 0.62658 lbf-sec^n/100ft^2)

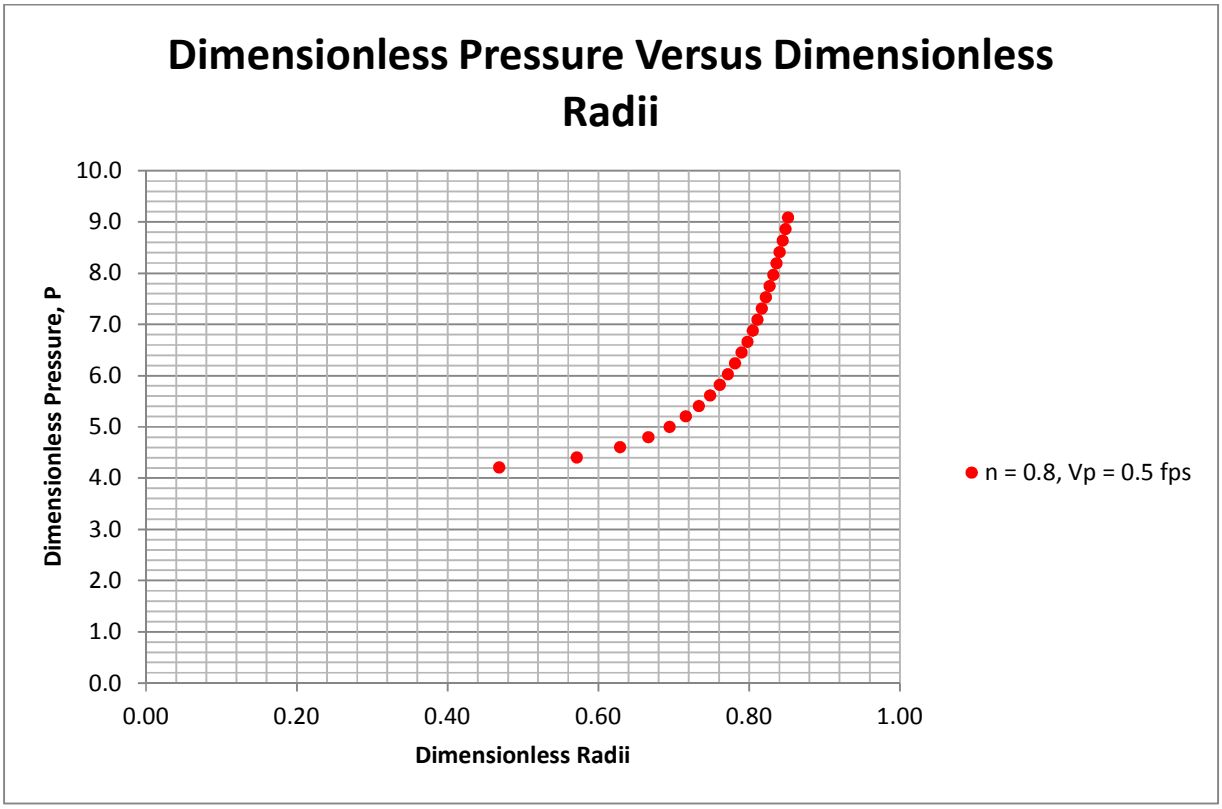

Figure 18: Graph of Dimensionless Pressure Versus Dimensionless Radii (For ε = 0.8, shear stress $_0$ = 10 lbf/100 ft^2, flow behavior index n =0.80, consistency index K = 0.0062658 lbf-sec^n/ft^2 = 0.62658 lbf-sec^n/100ft^2)

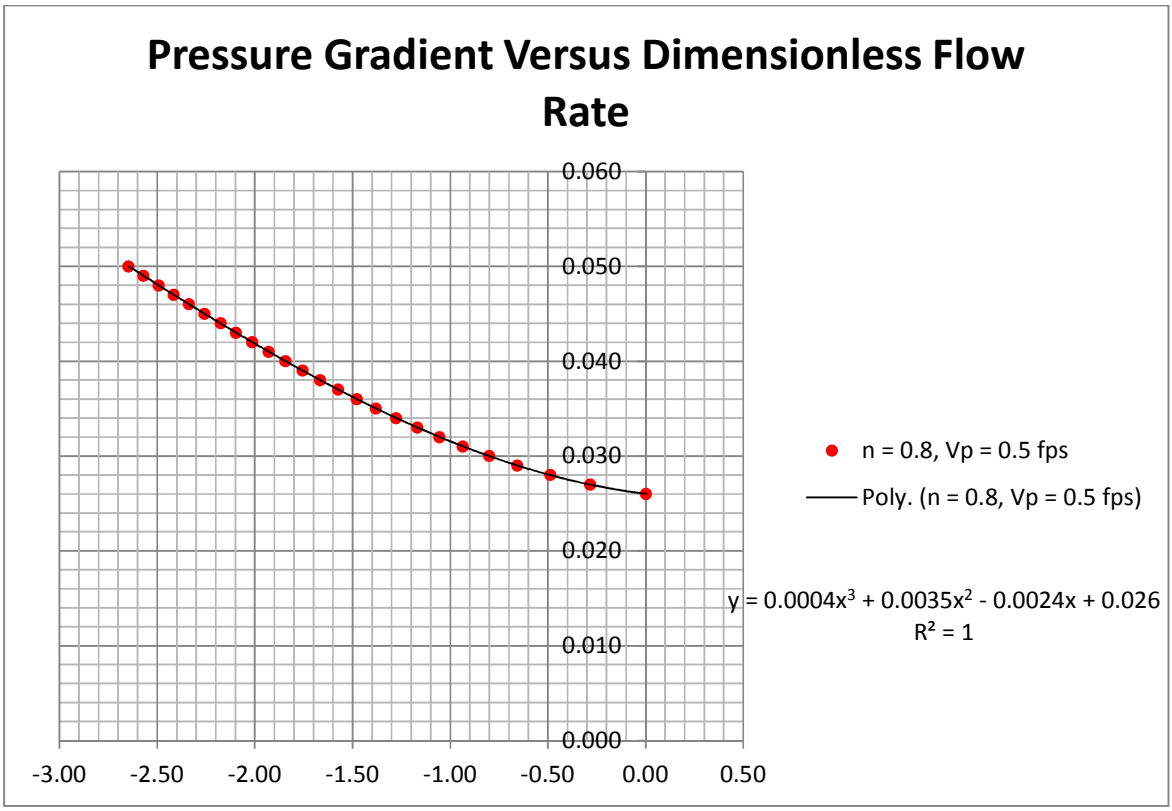

Figure 19: Graph of Pressure Gradient Versus Dimensionless Radii (For ε = 0.8, shear stress $_0$ = 10 lbf/100 ft^2, flow behavior index n =0.80, consistency index K = 0.0062658 lbf-sec^n/ft^2 = 0.62658 lbf-sec^n/100ft^2)

CHAPTER 6

CONCLUSIONS AND RECOMMENDATIONS

6.1 CONCLUSIONS

The following conclusions can be made based from the analysis showed above:

1) The Conformal Mapping - Slot Model Technique made a reasonable prediction for dimensionless pressure, which in turn can be used to evaluate the pressure gradient.
2) The dimensionless pressure profiles for the yield power law fluids in the annulus are therefore dependent on the specific shear stress of the given fluid, and as well on other fluid parameters such as consistency index behavior, and it also depends on the fluid index behavior.
3) The annular clearance is very important in the computation of surge and swab. As the annular clearance increases the surge pressure reduces and as the clearance reduces the surge increases.
4) It is possible to apply conformal mapping on eccentric annulus to map it to a concentric annulus and provide surge/swab pressure values for the eccentric annulus. This technique has not been used in literature before. This technique avoids the laborious mathematical computations involved in applying polar coordinate system to eccentric annulus.

RECOMMENDATIONS

Further recommended studies include:

1) Consider the case of unsteady flow of yield power law fluids , and the estimate of the corresponding surge and swab for concentric and eccentric annulus, as in real life situations where of fluid flow is unsteady.
2) Also a model can be developed for surge and swab pressure for an open end drill string, as the model developed in this paper is for closed drill string.
3) With respect to the yield power law fluid and eccentric annulus, the pipe velocity at which the tubular goods can be operated without fracturing the formation can be evaluated.

REFERENCES

Adam , T. B et al: Applied Drilling Engineering (1986), Society of Petroleum Engineers, Richardson Texas.

Bird, R. B. et al. Transport Phenomena, (1960), JOHN WILEY & SONS Inc.

Bizanti, M.S.; Felipe, R.E.: "Are Improved Surged Models Needed?" Society of Petroleum Engineers (1991) SPE 22057.

Burkhardt, J.A.: "Wellbore pressure surges produced by pipe movement," J. Pet. Tech. (June 1961), pp. 595-605.

Canon, G.E.: "Changes in hydrostatic pressure due to withdrawing drill pipe from the hole" API Drill and Prod. Pract. (1934) pp 42-47

Chukwu, G.A.; E.F. Blick: "Surge and swab pressure model: Surge and swab pressure from couette flow of power-law fluids through a concentric annulus," Pet. Eng. Int'l. (Nov. 1991)

Chukwu, G.A.; "Surge and swab pressure computed for couette flow of power-law fluids", Ph.D. Dissertation University of Oklahoma, (1989).

Chukwu, G. A: " A Practical Approach for Predicting Casing Running Speed from Couette Flow of Non-Newtonian Power-Law Fluids" Western Regional Meeting Bakersfield, (1995) Society of Petroleum Engineers, inc. pp. 263-268

Clark, E. H., Jr.: "Bottom-hole pressure surges while running pipes," Pet. Engr. Int. Vol.27 (Jan. 1955)

Crespo, F.; Ramadan A.: “Surge and Swab Pressure Predictions for Yield-Power-Law Drilling Fluids” SPE Latin American & Caribbean Petroleum Engineering Conference (December 2010)

Deniz, U.; Canan, O.; Ismall, T.: “Flow of Power Law Fluid in an Eccentric Annulus” SPE Drilling Engineering (Sept. 1989), pp. 269-272.

E.Perez , http://4dlab.info/article_what_are_conformal_mappings.htm

Fontenot, J.E. and Clark, R.K.: “An improved method for calculating pressures in a drilling well,” Soc. Pet. Eng. Jour., (Oct, 1974)

Goins, W.C.; J.P. Weichhert; J.L. Burba, Jr.; D.D. Dawson, Jr.; and A.J. Teplitz: “Down-the-hole pressure surges and their effect on loss of circulation,” API Drill and Prod. Pract. (1951), pp. 125-132.

Haciilamoglu, M; Langlinais, J: “Effect of Pipe Eccentricity on Surge Pressures” Journal of Energy Resources Technology (Sept. 1991), Vol 113/115

Horn, A. J.: “Well blowouts in California drilling operations, causes and suggestions for prevention,” API Drill and Prod. Pract. (1950), pp. 112-128.

Jeng-Tzong Chen; Ming-Hong Tsai; Chein-Shan Liu: “Conformal Mapping and Bipolar Coordinate for Eccentric Laplace Problems” J Appl Mech (Oct., 2008) pp 1-10.

Moore, P.L: Drilling Practices Manual, Tulsa, Pet. Publ. Co.; (1974), pp, 241-252

Mitchell, R.F.: “Dynamic surge/swab pressure predictions,” SPE Drilling Engineering (Sept. 1988), pp. 325-333.

Ozbayoglu, M. E.; C. Omurlu: “Analysis of the Effect of Eccentricity on Flow Characteristics of Annular Flow of Non-Newtonian Fluids using Finite Element Method” Society of Petroleum Engineers (2006)

Rudi Rubiandini R.S.: “New Formula of Surge Pressure for Determining Safe Trip Velocities” Society of Petroleum Engineers (October 2000).

Suman Ganguli: “Application of Conformal Mappings” Department of Physics, University of Tennessee, Knoxville. (November 20, 2008)

Wesley Pacheco C.; Bernado A.; Jesus Carlos du Mota; Leonardo da Cunha Brito. Marcel Wu, Aylton Jose A.; Luciano Martins W.; Carlos F.R.; “Electromagnetic Problems Solving by Conformal Mapping: A Mathematical Operator for Optimization” Mathematical Problems in Engineering Volume 2010 Article ID 742039

Yang, Liao; Chukwu, Godwin.A.; “ Application of coquette flow of Non-Newtonian Power-Law Fluids in Eccentric Annuli to Petroleum Engineering Problems” M.Sc Thesis, University of Alaska Fairbanks, (August 1993).

Yuejin, L.; Peden, J.M.: “Flow of Non-Newtonian Fluids through Eccentric Annulli” SPE Production Engineering (Feb. 1990), pp 91-96.